Kagomé- and triangular-lattice Heisenberg antiferromagnets: Ordering from quantum fluctuations and quantum-disordered ground states with unconfined bosonic spinons

Subir Sachdev

Center for Theoretical Physics, P.O. Box 6666, Yale University, New Haven, Connecticut 06511

(Received 23 October 1991)

The kagomé-lattice quantum Heisenberg antiferromagnet is studied by a large-N expansion based upon groups with symplectic $Sp(N)$ symmetry. Two distinct types of ground states are found. (i) For large values of the "spin" the ground state has long-range magnetic order with the spins ordered in a $\sqrt{3} \times \sqrt{3}$ structure with 9 sites per unit cell. Quantum fluctuations are explicitly shown to select this structure from the large number of classically degenerate states. The only zero-energy excitations about the magnetically ordered state are shown to be the physical, infinite-wavelength, Goldstone spin waves; in contrast the naive semiclassical theory has zero-energy spin waves at all wave vectors. (ii) For small values of the "spin," the ordered moment disappears and we obtain a quantum-disordered ground state with no broken symmetries. As in previous work on frustrated square-lattice antiferromagnets, this state is argued to possess unconfined, spin-$\frac{1}{2}$, bosonic, spinon excitations for all values of the underlying lattice spin. A similar, small-"spin" quantum-disordered ground state with unconfined bosonic spinons is studied in the triangular-lattice quantum Heisenberg antiferromagnet by extending earlier results. A large N, $Sp(N)$ theory of the classical kagomé Heisenberg antiferromagnet at finite temperature is also presented: fluctuations of the $\sqrt{3} \times \sqrt{3}$ structure dominate, with a correlation length which diverges exponentially in the zero-temperature limit. The significance of these results for experimental kagomé-lattice systems is discussed.

I. INTRODUCTION

Recent years have seen a flurry of interest on the properties of frustrated quantum Heisenberg antiferromagnets in two dimensions.[1–13] The interest is motivated partly by the search for quantum disordered ground states and their possible relationship to high temperature superconductivity.[14] Moreover, such ground states are interesting in their own right, as they can display new types of order and possess excitations with unusual quantum numbers. The structure of the magnetically ordered phases of such magnets (i.e., phases in which the expectation of the single spin operators $\langle S \rangle$ is nonzero) can also be nontrivial: in particular, the classical ground states of many such magnets have "accidental" degeneracies which are lifted by quantum fluctuations. The magnetic ordering is therefore induced by quantum fluctuations[15] ("order from disorder").

The kagomé-lattice quantum Heisenberg antiferromagnet has remained a particularly perplexing, but also interesting model.[16–20] There are several reasons for this.

(i) The classical kagomé Heisenberg antiferromagnet has a macroscopic ground-state entropy. One source of this entropy is the number of ways in which spins A, B, C (Fig. 1) pointing to the vertices of an equilateral triangle can be placed on the kagomé lattice with no two nearest neighbors pointing in the same direction. Furthermore, the spins on every closed loop consisting only of, e.g., B, C spins can be rotated freely about the axis defined by the A spins with no change in the energy. It is expected that these degeneracies will be lifted by thermal or quantum fluctuations.[15] The semiclassical theory expands about a saddle point with this large degeneracy; the nature of the expansion is therefore far from clear and its structure remains to be unraveled.

(ii) The sites have a low coordination number of 4 and the system is therefore an attractive candidate to display a quantum disordered ground state for spin $\frac{1}{2}$.

(iii) Two experimental realizations of the kagomé antiferromagnet have recently been proposed. These are the second layer of He^3 atoms on a graphite substrate[21,22]— where the spin $S = \frac{1}{2}$, and the kagomé nets of $S = \frac{3}{2}$ Cr moments in $SrCr_{8-x}Ga_{4+x}O_{19}$.[23–25]

A recently developed large-N expansion of frustrated quantum antiferromagnets[3,4] is particularly suited for clarifying the physics of the kagomé lattice antiferromagnet. The main reasons for this are the following

(i) The ordering effects of quantum fluctuations are included self-consistently in the large-N saddle point. There are no accidental degeneracies in the mean-field
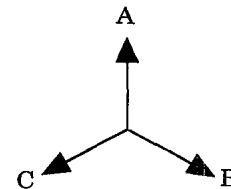

FIG. 1. The three spin directions A, B, C pointing toward the vertices of an equilateral triangle.

theory of the magnetically ordered phases. A related benefit is that *the only zero modes in the $1/N$ fluctuations about the magnetically ordered phases are the physical Goldstone spin-wave modes whose energy vanishes only in the long-wavelength limit.* This should be contrasted with the semiclassical expansion which has excitations with zero energy at all momenta;[16,18] it is then not clear, even in principle, of how a sensible semiclassical expansion can be defined.

(ii) The antiferromagnet undergoes a zero temperature phase transition at $N = \infty$ from a magnetically ordered phase to a quantum disordered phase as the value of the "spin" is varied. The "spin" appears as a parameter in the $N = \infty$ mean-field theory. The structure and excitations of the quantum disordered ground state, and its relationship to the magnetically ordered phase can be systematically studied.

We will now define the models studied and state the main new results of this paper. Details will be presented in the body of the paper. Readers not interested in how the results were obtained should read this section and then skip directly to Sec. VI, where we will compare our theoretical results with those of others and discuss implications for experiments.

We introduce canonical Bose operators b_i^α upon the sites i of the kagomé lattice, where the index $\alpha = 1, \ldots, 2N$ transforms under the symplectic group Sp (N).[3,4] We will of course be interested finally in the group SU(2) which is isomorphic to Sp(1). The constraint

$$b_{i\alpha}^\dagger b_i^\alpha = n_b \tag{1.1}$$

is imposed on every site i of the lattice to fix the representation of Sp(N) spin on every site. We have

$$n_b = 2S \quad \text{for SU(2)} . \tag{1.2}$$

We will examine the Hamiltonian

$$H_{\mathrm{AF}} = -\frac{J}{2N} \sum_{<ij>} (\mathcal{J}^{\alpha\beta} b_{i\alpha}^\dagger b_{j\beta}^\dagger)(\mathcal{J}_{\gamma\delta} b_i^\gamma b_j^\delta) , \tag{1.3}$$

where the sum over i, j extends over nearest neighbors on the kagomé lattice. The tensor $\mathcal{J}$ is the $2N \times 2N$ generalization of the ε tensor of SU(2)$\cong$Sp(1):

$$\mathcal{J}_{\alpha\beta} = \mathcal{J}^{\alpha\beta} = \begin{pmatrix} & 1 & & & \\ -1 & & & & \\ & & & 1 & \\ & & -1 & & \\ & & & & \ddots \\ & & & & & \ddots \end{pmatrix} . \tag{1.4}$$

For the special case of $N = 1$, it can be shown using Eq. (1.1) that

$$(\mathcal{J}^{\alpha\beta} b_{i\alpha}^\dagger b_{j\beta}^\dagger)(\mathcal{J}_{\gamma\delta} b_i^\gamma b_j^\delta) = -2\mathbf{S}_i \cdot \mathbf{S}_j + n_b^2/2 + \delta_{ij} n_b , \tag{1.5}$$

where $\mathbf{S}_i = b_{i\alpha}^\dagger \tau_\beta^\alpha b_i^\beta/2$, with τ the Pauli matrices, are the usual SU(2) spin operators. The H_{AF} becomes the

familiar bilinear, nearest-neighbor, Heisenberg Hamiltonian plus constants. The large-N limit of H_{AF} is taken with[3,4,26]

$$\kappa = \frac{n_b}{N} \quad \text{fixed} . \tag{1.6}$$

For large values of κ the system is magnetically ordered, while the quantum disordered phases appear at small κ.

An important property of the zero temperature, $N = \infty$ mean-field theory is its behavior at large κ. It has been shown (Ref. 4 and Sec. II) that properties of the single point $N \to \infty$ at fixed κ followed by $\kappa \to \infty$, are identical to the classical point which is $n_b \to \infty$ at fixed N. However the region $N \to \infty$ at fixed but large κ is quite different from the semiclassical region which is n_b large and N fixed. One of the main points of this paper is to demonstrate usefulness of the former region in understanding ordering due to quantum fluctuations.

We are now ready to state the main new results of this paper.

A. Quantum kagomé antiferromagnet

The large-N kagomé quantum Heisenberg antiferromagnet has two types of ground states.

1. Magnetically ordered ground state

This occurs for $\kappa > 0.53$ at $N = \infty$, with the orientation of the spin-condensate shown in Fig. 2. The spin arrangement forms a triangular lattice with a unit cell of 9 sites. This state has been considered earlier in Refs. 16 and 18 as the ground state of the semiclassical limit of the kagomé lattice antiferromagnet with first and second neighbor interactions; following them we will refer to it as the $\sqrt{3} \times \sqrt{3}$ state. The "classical" limit ($\kappa = \infty$) of this state has a huge degeneracy associated with (i) rearrangement of the A, B, C spins among all the ground states of the 3-state Potts antiferromagnet on the kagomé lattice and (ii) independent rotation of the two spin species around any hexagon about the axis parallel to the third spin species. In Sec. V we will explicitly cal-
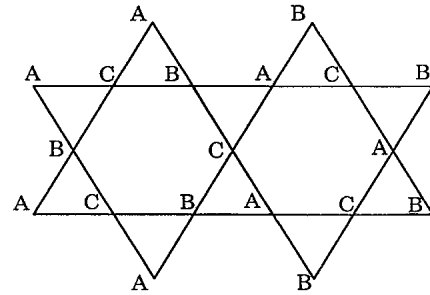

FIG. 2.   Spontaneous magnetization of the ground ($\sqrt{3} \times \sqrt{3}$) state of the kagomé-lattice quantum antiferromagnet. There are 9 sites per unit cell. Suitably oriented spins can be added to the center of every hexagon to yield the ground state of the triangular lattice antiferromagnet. This state has the link variables $Q_1 = -Q_2$ (Sec. IV).

culate the energy associated with these deformations of the ground state at finite, but large κ values: we find that the energy is nonzero, positive, and of order N. Thus the only remaining degeneracy of the $\sqrt{3} \times \sqrt{3}$ ground state is that due to a single uniform global rotation.

We have also computed the staggered moment $\mathcal{M}$ in the ground state as a function of κ at $N = \infty$; we find

$$\frac{\mathcal{M}}{N\kappa} = 1 - \frac{0.53}{\kappa} + \mathcal{O}\left(\frac{1}{N}\right) . \tag{1.7}$$

The first two terms are the complete result at $N = \infty$, and not an expansion in powers of $1/\kappa$. All remaining terms will involve subleading powers of $1/N$. We emphasize that this staggered moment does not include contributions from quantum fluctuations to the sectors associated with other states which are degenerate in the classical limit: quantum fluctuations endow these states with energy differences of order N and they can therefore be neglected in the large-N limit. For finite N, tunneling between these classically degenerate states will presumably lead to some reduction of the moment. For sufficiently large N however, the moment is expected to remain finite in the limit $\kappa \to \infty$.

Another magnetically ordered state with an energy close to, but higher than, the $\sqrt{3} \times \sqrt{3}$ state was found and is shown in Fig. 3. The unit cell of the spins is the same as that of the lattice: it is therefore referred to as the $\mathbf{k} = 0$ state. All the other spin configurations associated with the remaining ground states of the 3-state Potts antiferromagnet have an energy intermediate between the $\sqrt{3} \times \sqrt{3}$ and the $\mathbf{k} = 0$ states.

2. Quantum disordered ground state

For $\kappa < 0.53$, the spin condensate disappears and the $\mathrm{Sp}(N)$ symmetry is restored. The resulting state also does not break any additional symmetries: parity, time reversal, and lattice translational symmetries are all preserved. It is therefore different from the quantum-disordered ground states of models with collinear magnetically ordered states,[3,4,27,28] which have spin-Peierls order with a broken lattice translational symmetry. The excitation spectrum has a gap. The low-lying excitations are spin-$\frac{1}{2}$ bosonic spinons which carry a unit charge of

FIG. 4. Momentum dependence of the energy, $\omega(\mathbf{k})$ of the lowest excited spinon state for the quantum-disordered ground state (which has $Q_1 = -Q_2$) of the kagomé-lattice quantum antiferromagnet at $\kappa = 0.35$. The energy is measured in units of $J/2$, and a is the nearest-neighbor spacing on the kagomé lattice. The minimum excitations are the spinons at $\mathbf{k} = \mathbf{k}_1 = (2\pi/3a)(1,0)$ and $\mathbf{k} = \mathbf{k}_2 = (2\pi/3a)(-1,0)$ and other points separated from $\mathbf{k}_1, \mathbf{k}_2$ by vectors of the reciprocal lattice (here a is the nearest-neighbor spacing on the kagomé lattice).

an internal compact U(1) gauge force. We examine the structure of the U(1) gauge theory and find, in a manner similar to Refs. 3 and 4, that the condensation of charge-2 Higgs scalars quenches the U(1) gauge force and the spinons remain unconfined. These free spin-$\frac{1}{2}$ spinons occur for all values of the underlying spin n_b. Thus a system with integer "spin" $n_b/2 = 1$ can possess spinor excitations. The spectrum of the spinons is shown in Fig. 4. With our particular gauge choice, the spinons with minimum excitations are at $\mathbf{k} = \mathbf{k}_1 = (2\pi/3a)(1,0)$ and $\mathbf{k} = \mathbf{k}_2 = (2\pi/3a)(-1,0)$ and other points separated from $\mathbf{k}_1, \mathbf{k}_2$ by vectors of the reciprocal lattice (here a is the nearest-neighbor spacing on the kagomé lattice). The nature of the spin correlations in the ground state can be determined by examining the structure factor (the equal-time spin-spin correlation function). The $N = \infty$ result for the structure factor is shown in Fig. 5. The global maxima of the structure factor are at six wave vectors with magnitude $4\pi/(3a)$.
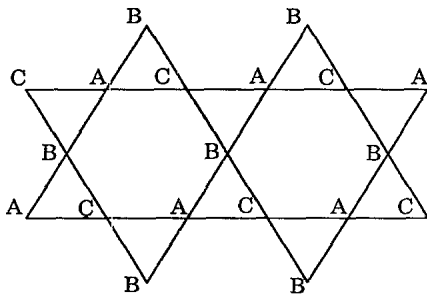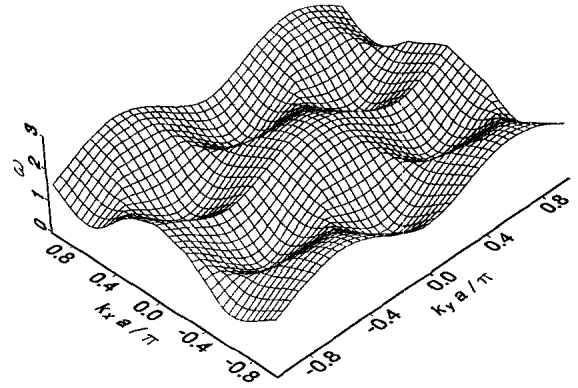

FIG. 3. Spontaneous magnetization of the $\mathbf{k} = 0$ state of the kagomé-lattice quantum antiferromagnet at zero temperature. Its energy is higher than the state in Fig. 2. This state has the link variables $Q_1 = Q_2$ (Sec. IV).
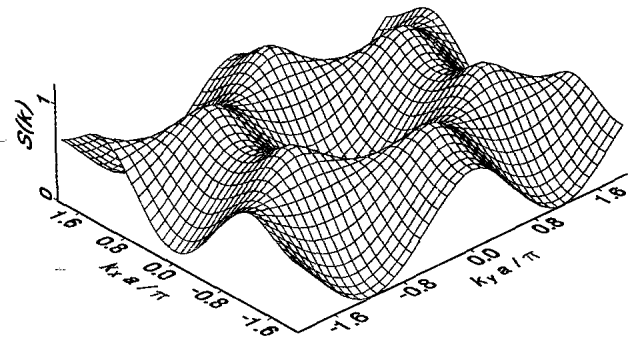

FIG. 5. Zero-temperature structure factor, $S(\mathbf{k})$ of the quantum-disordered ground state ($Q_1 = -Q_2$) of the kagomé-lattice quantum antiferromagnet at $\kappa = 0.35$ and $N = \infty$. The global maxima are at six wave vectors with magnitude $4\pi/(3a)$. $S(\mathbf{k})$ is computed from Eqs. (2.17) and (2.18).

Following Refs. 3 and 4 we note that this quantum-disordered ground state (and the quantum-disordered ground states of frustrated antiferromagnets on the square lattice with incommensurate spin correlations found in Refs. 3 and 4) is an explicit counterexample to Laughlin's "fractional quantization principal."[29] This principal asserts that the free spin-$\frac{1}{2}$ excitations of "spin-fluid" states must obey fractional statistics. The present quantum disordered state is evidently a spin fluid; it has free spin-$\frac{1}{2}$ spinons which are *bosons*.[3,4]

B. Quantum triangular antiferromagnet

The present large-N method[3,4] can also be applied to the triangular-lattice quantum Heisenberg antiferromagnet. A closely related mean-field theory has already been studied.[11] We will review and extend their results to obtain the following.

(a) A magnetically ordered ground state with the usual three-sublattice condensate polarization, which is stable for $\kappa > 0.34$, and has a staggered moment

$$\frac{\mathcal{M}}{N\kappa} = 1 - \frac{0.34}{\kappa} + \mathcal{O}\left(\frac{1}{N}\right) \qquad (1.8)$$

and

(b) a quantum-disordered ground state for $\kappa < 0.34$ which is very similar to the kagomé lattice quantum-disordered state: i.e., it has massive, spin-$\frac{1}{2}$, unconfined, bosonic spinons. The structure of this state clearly disagrees with the Laughlin-Kalmeyer[12] state on the triangular lattice which was argued to possess semionic spinons. As above, these results are also a counterexample to Laughlin's fractional quantization principal.[29]

C. Classical kagomé antiferromagnet

Finally, the Sp(N) large-N approach was also used to study thermal fluctuations in the *classical* Heisenberg antiferromagnet on a kagomé lattice; details are presented in the Appendix. Because this is a two-dimensional classical system with a non-Abelian continuous symmetry, no long-range or quasi-long-range order can be present at any nonzero temperature. However, we find that thermal fluctuations select configurations which have short-range order of the $\sqrt{3} \times \sqrt{3}$ structure (Fig. 2), in agreement with the high-temperature expansion of Ref. 18. The correlation length of the $\sqrt{3} \times \sqrt{3}$ structure diverges as $\exp(c/T)$ as the temperature $T \to 0$. We have also calculated the structure factor of the classical antiferromagnet in the large-N limit: the result is shown in Fig. 6. Note that it is similar to the structure factor of quantum-disordered ground state in Fig. 5 and has six peaks at wave vectors with magnitude $4\pi/(3a)$. Recall that the high-temperature expansion of this model had to include terms of order $1/T^8$ before obtaining a qualitatively similar momentum dependence in the structure factor;[18] in contrast, the momentum dependence is present in the leading term of the symplectic large-N approach.

The outline of the rest of the paper is as follows. The general structure of the Sp(N) large-N limit is reviewed
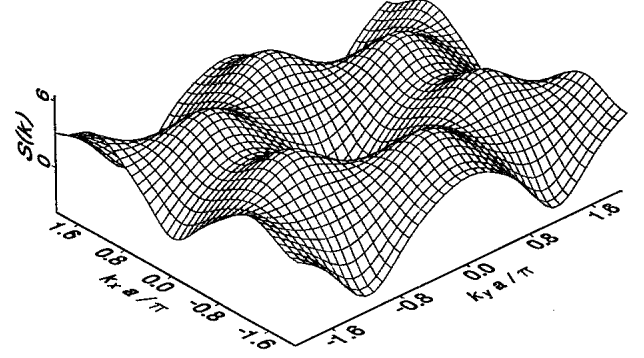

FIG. 6. Large-N result for the structure factor, $S(\mathbf{k})$ of the classical antiferromagnet on the kagomé lattice at a temperature $T = 0.225J$. The mean-field free-energy is minimized by link variables $Q_1 = -Q_2$ (see the Appendix). The global maxima are at six wave vectors with magnitude $4\pi/(3a)$. Notice that $S(\mathbf{k})$ becomes negative at some values of $\mathbf{k}$; this is possible because the expression for the structure factor [Eq. (2.18)] is positive definite only at $N = 2$.

in Sec. II. Readers not interested in technical details may skip this section. The large-N theory is first applied to the triangular quantum lattice in Sec. III: this allows us to display its general features without the additional technical complications present in the kagomé lattice. The results are then extended to the kagomé lattice in Sec. IV: the magnetically ordered and quantum disordered ground states discussed above are found. The selection of the magnetically ordered ground state by quantum fluctuations in the kagomé lattice is studied in greater detail in Sec. V. Finally the main results are recapitulated and compared with previous theoretical investigations in Sec. VI. Implications for the experiments[21−25] are also presented in Sec. VI. An appendix contains results from the large-N theory of the thermal fluctuations in the classical Heisenberg antiferromagnet on the kagomé lattice.

II. GENERAL FORMALISM

In this section we review the large-N expansion technique for an arbitrary quantum Heisenberg antiferromagnet at zero temperature. Some of this has already been presented in Ref. 4 and is repeated here for completeness. We will consider a general Hamiltonian of the form

$$H_{\text{AF}} = -\frac{1}{2N} \sum_{i>j} J_{ij} (\mathcal{J}^{\alpha\beta} b_{i\alpha}^{\dagger} b_{j\beta}^{\dagger})(\mathcal{J}_{\gamma\delta} b_i^{\gamma} b_j^{\delta}) , \qquad (2.1)$$

where the sum over i, j extends over the sites of an arbitrary lattice. The constraint (1.1) is imposed on every site of the lattice.

The large-N limit of H_{AF} is taken with κ fixed to an arbitrary value. Depending upon the values of the J_{ij} and of κ, the ground state of H_{AF} may either break global Sp(N) symmetry and possess magnetic long-range order (LRO) or be Sp(N) invariant with only short-range order (SRO) in the two-spin correlation function; the latter case does not exclude the possibility of other types

of order associated with the breaking of lattice or time-reversal symmetries. We will keep the discussion of the large-N limit general by allowing for the possibility of LRO. We begin by introducing the parametrization

$$b_i^{m\sigma} \equiv \begin{pmatrix} \sqrt{N} x_i^\sigma \\ \tilde{b}_i^{\tilde{m}\sigma} \end{pmatrix} . \tag{2.2}$$

We have introduced a natural double-index notation $\alpha \equiv (m,\sigma)$ with $m = 1,\ldots,N$ and $\sigma = \uparrow, \downarrow$. The index $\tilde{m} = 2,\ldots,N$. The x^σ field has been introduced to al-

low for a nonzero condensate $\langle b_i^{m\sigma} \rangle = \sqrt{N} \delta_1^m x_i^\sigma$; we will only consider models in which the condensate in the LRO phase can be transformed by a uniform global Sp(N) rotation into this form. We will also not explicitly consider the fluctuation of the $m = 1$ component of $b_i^{m\sigma}$ because its contribution is much smaller than those from the remaining $N - 1$ components for large N—see also the end of Sec. II B. We insert (2.2) into H_{AF}, decouple the terms quartic in b by Hubbard-Stratanovich fields $Q_{ij} = -Q_{ji}$, and enforce the constraints by the Largrange multipliers λ_i. This yields

$$H_{\text{MF}} = \sum_{i>j} \left[N \frac{J_{ij}|Q_{ij}|^2}{2} - \frac{J_{ij}Q_{ij}}{2} \varepsilon_{\sigma\sigma'} \left(N x_i^\sigma x_j^{\sigma'} + \sum_{\tilde{m}} \tilde{b}_i^{\tilde{m}\sigma} \tilde{b}_j^{\tilde{m}\sigma'} \right) + \text{H.c.} \right]$$
$$+ \sum_i \lambda_i \left(N |x_i^\sigma|^2 + \sum_{\tilde{m}\sigma} \tilde{b}_{i,\tilde{m}\sigma}^\dagger \tilde{b}_i^{\tilde{m}\sigma} - n_b \right) . \tag{2.3}$$

The large-N limit is obtained by integrating over the $2(N-1)$ b fields. The resulting effective action, expressed in terms of the Q_{ij}, λ_i, and x_i^σ fields, will have a prefactor of N (and some terms of order 1 which are subdominant) and is therefore well approximated by its saddle-point value. The Q, λ, x fields are expected to be time independent at the saddle point and this is implicitly assumed in the following. The functional integral over the b requires knowledge of the eigenmodes of H_{MF}. Let us collect the terms in H_{MF} dependent on the b and write them in the compact form

$$H_{\text{MF}} = \sum_{r,s} \Psi_r^\dagger D_{rs} \Psi_s + \cdots , \tag{2.4}$$

where the ellipses denote terms independent of the $\tilde{b}$,

$$\Psi = \begin{pmatrix} \tilde{b}_i^\uparrow \\ \tilde{b}_{i\downarrow}^\dagger \end{pmatrix} , \tag{2.5}$$

the indices r, s run over the pair of site-spin indices (i, σ), and D is a $2N_s \times 2N_s$ (N_s = number of sites in the system) Hermitian matrix given by

$$(D)_{ij} = \begin{pmatrix} \lambda_i \delta_{ij} & -J_{ij} Q_{ij}^*/2 \\ J_{ij} Q_{ij}/2 & \lambda_i \delta_{ij} \end{pmatrix} . \tag{2.6}$$

We have also temporarily suppressed the index $\tilde{m}$ as all the terms are diagonal in it. The Ψ operators satisfy the commutation relations

$$[\Psi_r, \Psi_s^\dagger] = \tau_{rs}^3 , \tag{2.7}$$

where

$$(\tau^3)_{ij} = \begin{pmatrix} 1 & 0 \\ 0 & -1 \end{pmatrix} . \tag{2.8}$$

We now attempt diagonalization of H_{MF} by performing a suitable linear transformation on Ψ. We introduce the $2N_s$ operators Γ

$$\Gamma = \begin{pmatrix} \gamma_\mu^\uparrow \\ \gamma_{\mu\downarrow}^\dagger \end{pmatrix} \tag{2.9}$$

with $\mu = 1,\ldots,N_s$, which are related to Ψ by the linear transformation

$$\Psi = M\Gamma . \tag{2.10}$$

The Γ will satisfy the canonical commutation relations (2.7), and also diagonalize H_{MF} provided

$$M^\dagger D M = \hat{\omega} , \quad M^\dagger \tau^3 M = \tau^3 , \tag{2.11}$$

where $\hat{\omega}$ is a diagonal matrix of the bosonic eigenenergies. Equations (2.11) can be combined to yield

$$\tau^3 D M = M \tau^3 \hat{\omega} . \tag{2.12}$$

In other words, the columns of M are the eigenvectors of the non-Hermitian matrix $\tau^3 D$ and the diagonal elements of $\tau^3 \hat{\omega}$ are the corresponding eigenvalues. The special form of D in Eq. (2.6) and the antisymmetry of Q_{ij} can be used to show that the eigenvalues occur in pairs with opposite signs ($\omega_\mu, -\omega_\mu$), where we choose $\omega_\mu \geq 0$, and that M has the form

$$M = \begin{pmatrix} U & -V^* \\ V & U^* \end{pmatrix} , \tag{2.13}$$

where the U, V are $N_s \times N_s$ matrices. The ω_μ are clearly the spectrum of Bose-particlelike spinon excitations above the ground state, and the U, V their wave functions.

Finally, we insert the bosonic eigenmodes into H_{MF} and obtain the ground-state energy, E_{MF}

$$\frac{E_{\text{MF}}}{N} = \sum_{i>j} \left(\frac{J_{ij}|Q_{ij}|^2}{2} - \frac{J_{ij}Q_{ij}}{2} \varepsilon_{\sigma\sigma'} x_i^\sigma x_j^{\sigma'} + \text{H.c.} \right)$$
$$+ \sum_i \lambda_i (|x_i^\sigma|^2 - 1 - \kappa) + \sum_\mu \omega_\mu(Q, \lambda) . \tag{2.14}$$

In the last term we have emphasized that the ω_μ depend upon Q, λ. Finding the ground state of H_{AF} in the large-N limit is now reduced to the problem of minimizing E_{MF} with respect to the independent variables Q_{ij}, x_i^σ with the λ_i chosen such that the constraints

$$\frac{\partial E_{MF}}{\partial \lambda_i} = 0 \tag{2.15}$$

are always satisfied. It is instructive to examine the equations obtained by demanding stationarity of E_{MF} with respect to x_i^σ:

$$-\sum_j \varepsilon_{\sigma\sigma'} \frac{J_{ij} Q_{ij}}{2} x_j^{\sigma'} + \lambda_i x_{i\sigma}^* = 0 . \tag{2.16}$$

This equation has two possible solutions.

(i) $x_i^\sigma = 0$: this gives the SRO in the two-spin correlation function.

(ii) $x_i^\sigma \neq 0$: these are the phases with magnetic LRO and occur for large values of κ. Comparing Eq. (2.16) with Eqs. (2.6) and (2.12) we see that this condition is equivalent to demanding that at least one of the $\omega_\mu = 0$. These are the Goldstone modes associated with the $Sp(N)$ symmetry breaking.

A. Structure factor

An important experimental characterization of any ground state of H_{AF} is its structure factor $S(\mathbf{k})$. For the group SU(2) this is given by the equal-time spin-spin correlation function

$$S(\mathbf{k}) = \frac{1}{N_s} \sum_{i,j} \langle \mathbf{S}_i \cdot \mathbf{S}_j \rangle e^{i\mathbf{k} \cdot (\mathbf{r}_i - \mathbf{r}_j)} . \tag{2.17}$$

For $Sp(N)$, we must replace the right-hand side (rhs) by one of the infinite number of $Sp(N)$ invariants which reduce to $\mathbf{S}_i \cdot \mathbf{S}_j$ at $N = 1$. To choose among them impose the following criteria.

(i) The invariant must reduce to exactly $\mathbf{S}_i \cdot \mathbf{S}_j$ at $N = 1$ with no additional constants;

(ii) it has no disconnected component, i.e., its expectation value must vanish exactly for all N as $|\mathbf{r}_i - \mathbf{r}_j| \to \infty$ in a quantum disordered phase—a disconnected piece can arise from the i, j independent term in Eq. (1.5), $n_B^2/2$, if suitable factors of $1/N$ are not inserted in the generalization to arbitrary N; and

(iii) the sum rule on $\sum_{\mathbf{k}} S(\mathbf{k})$ is satisfied exactly by the leading order term as $N \to \infty$. A little experimentation shows that there is indeed a unique invariant satisfying these criteria:

$$\mathbf{S}_i \cdot \mathbf{S}_j \to \frac{1}{4N^2} (b_{i\alpha}^\dagger b_i^\beta b_{j\beta}^\dagger b_j^\alpha - \mathcal{J}^{\alpha\gamma} \mathcal{J}_{\beta\delta} b_{i\alpha}^\dagger b_i^\beta b_{j\gamma}^\dagger b_j^\delta) . \tag{2.18}$$

It is easy to show that structure factor satisfies the sum rule

$$\frac{1}{N_s} \sum_{\mathbf{k}} S(\mathbf{k}) = \frac{\kappa(\kappa + 2)}{4} . \tag{2.19}$$

As expected, there are no $1/N$ corrections to the sum

rule. The discrepancies of factors of $\frac{3}{2}$ which plagued earlier mean-field theories[26,11] have therefore been removed. Finally, we can use the expressions in Eqs. (2.9), (2.10), and (2.13) for the bosonic eignmodes of H_{MF} to obtain the $N \to \infty$ limit of the $T = 0$ structure factor in a quantum disordered phase:

$$S(\mathbf{k}) = \frac{1}{N_s} \sum_{i,j} e^{i\mathbf{k} \cdot (\mathbf{r}_i - \mathbf{r}_j)} \left(\sum_{\mu\nu} V_{i\mu} U_{i\nu} V_{j\mu}^* U_{j\nu}^* - \left| \sum_\mu V_{i\mu} U_{j\mu}^* \right|^2 \right) . \tag{2.20}$$

B. Large-κ limit

We now examine the large $\kappa = n_b/N$ limit of H_{MF} at zero temperature. Note that this limit corresponds to studying H_{AF} in the limit $N \to \infty$ with κ fixed, followed subsequently with the limit $\kappa \to \infty$. It is quite distinct from the classical limit which is $n_b \to \infty$ with N fixed. Nevertheless, as we will show below, the structure of the system at the limit point of $N \to \infty$ followed by $\kappa \to \infty$ is identical to the classical system obtained by $n_b \to \infty$. In particular, any ground-state degeneracies present in the classical system will also appear in the $\kappa \to \infty$ of H_{MF}. However the *semiclassical*, i.e., large n_b, fixed N, properties of H_{AF} will be quite distinct from those at $N \to \infty$, large κ. An advantage of the latter limit is that the properties of H_{AF} in the limit $N \to \infty$, i.e., H_{MF} can be determined to all orders in $1/\kappa$. In addition, order-by-disorder effects can be treated directly in the mean-field description of H_{MF}. In contrast, many of these effects only appear at some high order in $1/n_b$ in the semiclassical limit.

Let us now obtain an expansion of the properties of H_{MF} in inverse powers of κ. It is easy to show that for large κ, $Q_{ij} \sim \lambda_i \sim \kappa$ while $x_i^\sigma \sim \sqrt{\kappa}$. The leading term in E_{MF}/N is therefore of order κ^2. We therefore write

$$\frac{E_{MF}}{N} = E_c + E_1 + \cdots , \tag{2.21}$$

where E_c is of order κ^2, and E_1 is of order κ and lower-order terms have been omitted. From Eq. (2.14) we find that E_c is given by the minimization of

$$E_c = \sum_{i>j} \left(\frac{J_{ij}|Q_{ij}|^2}{2} - \frac{J_{ij} Q_{ij}}{2} \varepsilon_{\sigma\sigma'} x_i^\sigma x_j^{\sigma'} + \text{H.c.} \right) + \sum_i \lambda_i (|x_i^\sigma|^2 - \kappa) . \tag{2.22}$$

The minimization of E_c with respect to Q_{ij} is straightforward and yields $Q_{ij} = Q_{ij}^c$ where

$$Q_{ij}^{c*} = \varepsilon_{\sigma\sigma'} x_i^\sigma x_j^{\sigma'} . \tag{2.23}$$

Inserting this into Eq. (2.22) we obtain

$$E_c = -\sum_{i>j} \frac{J_{ij}}{2} |\varepsilon_{\sigma\sigma'} x_i^\sigma x_j^{\sigma'}|^2 + \sum_i \lambda_i (|x_i^\sigma|^2 - \kappa) . \tag{2.24}$$

It should now be obvious that the minimization of E_c with respect to x_i^σ and λ_i is completely equivalent to determining the classical ground states of the Hamiltonian $H_{\rm AF}$ for SU(2); by substituting Eq. (1.5) in Eq. (2.1) the dependent variables become vectors of length κ. Of particular interest in this paper are the cases where the classical solution has degeneracies in addition to those induced by globally uniform SU(2) rotations. Let $x_i^{\sigma c}$ and λ_i^c represent one such solution. Then it is not difficult to show that the first quantum correction, E_1, to $E_{\rm MF}$ in Eq. (2.21) is

$$E_1 = \sum_\mu \omega_\mu(Q^c, \lambda^c) - \sum_i \lambda_i^c , \qquad (2.25)$$

where Q^c is determined by inserting $x_i^\sigma = x_i^{\sigma c}$ in Eq. (2.23). In other words, the first quantum correction is simply given by the sum of the eigenfrequencies of bosons hopping via the Q_{ij} determined by the classical solution. We will find that this correction is usually sufficient to break the accidental classical degeneracies and select a particular ground state—an example of ordering induced by quantum fluctuations.

An objection might be raised that this ordering appears to be entirely due to the quantum fluctuations of the $N - 1$ transverse modes and is therefore absent for Sp($N = 1$). However we may include the fluctuation contribution from the $m = 1$ component by writing $b_i^{1\sigma} = x_i^{\sigma c} + \tilde{b}_i^{1\sigma}$; the resulting action will begin with terms quadratic in the $\tilde{b}_i^{1\sigma}$ as $x_i^\sigma = x_i^{\sigma c}$, $Q_{ij} = Q_{ij}^c$, and $\lambda_i = \lambda_i^c$ is a stationary point. Integrating out the $\tilde{b}_i^{1\sigma}$ we find a quantum correction to the energy which is identical in form to Eq. (2.25) and thus leads to the same ordering effects. Thus, carrying out the analysis in this subsection directly at $N = 1$ would have led to the same result for E_1. Of course, the inclusion of the fluctuations of the $b_i^{1\sigma}$ while neglecting the fluctuations of the Q_{ij} and λ_i, can only be justified by appealing to the large-N limit considered here.

III. TRIANGULAR-LATTICE QUANTUM ANTIFERROMAGNET

This section begins by reviewing the results of Yoshioka and Miyazaki, and Kol and Read[11] on the triangular-lattice quantum Heisenberg antiferromagnet using the notation of Sec. II. We will then systematically investigate the structure of the fluctuations about the mean-field theory. This will also serve as a useful warm-up for the more complex problem of the kagomé lattice antiferromagnet. We will begin in Sec. III A by studying first the quantum-disordered ground state which occurs at small values of κ. The large-κ ground state, which has magnetic long-range order will be examined in Sec. III B.

A. Quantum-disordered ground state

In this phase we have $x_i^\sigma = 0$. Thus our problem is reduced to determining the best configuration of the Q_{ij} and λ_i which minimize $E_{\rm MF}$ on the triangular lattice. From Ref. 11 we anticipate that all the $|Q_{ij}| = Q$ inde-
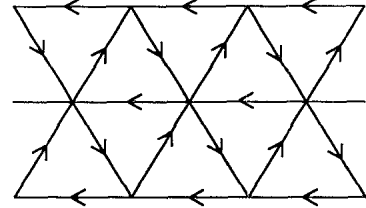

FIG. 7. Configurations of the Q_{ij} on the triangular lattice with nearest-neighbor spacing a. There is only one independent link variable Q, with the sign positive in the direction of the arrow. The $\lambda_i = \lambda$ on all sites.

pendent of i, j; the Q_{ij} can be chosen real, with signs as shown in Fig. 7. We also have $\lambda_i = \lambda$ independent of i. The eigenvalue equation (2.12) can be solved by a Fourier transform and we obtain the spectrum

$$\omega(\mathbf{k}) = [\lambda^2 - J^2 Q^2(\sin k_1 + \sin k_2 + \sin k_3)^2]^{1/2} ,$$
$$(3.1)$$

where the momentum $\mathbf{k}$ ranges over the first Brillouin zone of the triangular lattice and

$$k_p = \mathbf{k} \cdot \hat{\mathbf{e}}_p \qquad (3.2)$$

with the $\hat{\mathbf{e}}_p$ being vectors of length a pointing to the vertices of an equilateral triangle:

$$\hat{\mathbf{e}}_1 = a(\tfrac{1}{2}, \sqrt{3}/2) ,$$
$$\hat{\mathbf{e}}_2 = a(\tfrac{1}{2}, -\sqrt{3}/2) , \qquad (3.3)$$
$$\hat{\mathbf{e}}_3 = a(-1, 0) .$$

The ground-state energy is determined from Eq. (2.14) to be

$$\frac{E_{\rm MF}}{N N_s} = \frac{1}{N_s} \sum_{\mathbf{k}} \omega(\mathbf{k}) + \frac{3 J Q^2}{2} - \lambda(1 + \kappa) . \qquad (3.4)$$

The next step was a numerical minimization of $E_{\rm MF}$ with respect to Q subject to the condition

$$\frac{\partial E_{\rm MF}}{\partial \lambda} = 0 . \qquad (3.5)$$

A stable quantum disordered phase, with no broken symmetries, was found for $\kappa > 0.34$ and its energy is shown

TABLE I. Triangular-lattice quantum antiferromagnet: mean-field ground-state energies, $E_{\rm MF}/(J N N_s/2)$ as a function of $\kappa = n_B/N$. The state has magnetic long-range order for $\kappa > 0.34$

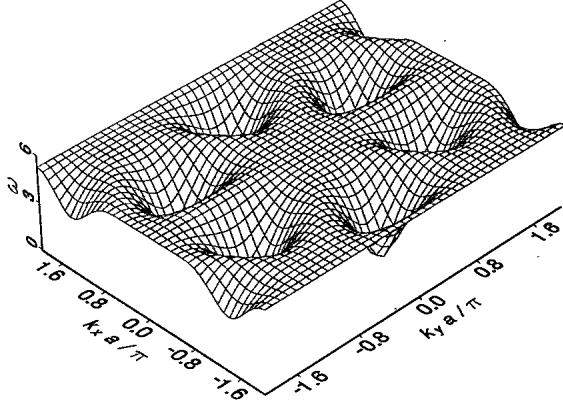| κ	$E_{\rm MF}/(J N N_s/2)$
0.1	−0.113
0.2	−0.257
0.3	−0.435
0.4	−0.656
0.5	−0.921
0.75	−1.782
1.00	−2.924
1.25	−4.347
1.50	−6.051

FIG. 8. Momentum dependence of the energy, $\omega(\mathbf{k})$ of the lowest excited spinon state for the quantum-disordered ground state of the triangular-lattice quantum antiferromagnet at $\kappa = 0.25$. The minimum excitations are the spinons at $\mathbf{k} = \tilde{\mathbf{k}}_1 = (4\pi/3a)(1,0)$ and $\mathbf{k} = \tilde{\mathbf{k}}_2 = (4\pi/3a)(-1,0)$ and other points separated from $\tilde{\mathbf{k}}_1, \tilde{\mathbf{k}}_2$ by vectors of the reciprocal lattice.

as a function of κ in Table I.

The mean-field excited states are given by the bosonic eigenfrequencies $\omega(\mathbf{k})$; these are shown in Fig. 8 at $\kappa = 0.25$. The minimum-energy excitations are the spinons at $\mathbf{k} = \tilde{\mathbf{k}}_1 = (4\pi/3a)(1,0)$ and $\mathbf{k} = \tilde{\mathbf{k}}_2 = (4\pi/3a)(-1,0)$ and other points separated from $\tilde{\mathbf{k}}_1, \tilde{\mathbf{k}}_2$ by vectors of the reciprocal lattice generated by $\tilde{\mathbf{G}}_1 = (4\pi/\sqrt{3}a)(0,1)$ and $\tilde{\mathbf{G}}_2 = (4\pi/\sqrt{3}a)(\sqrt{3}/2, -\frac{1}{2})$. We have also computed the spin structure factor, $S(\mathbf{k})$ using Eq. (2.20): the result is shown Figs. 9 at $\kappa = 0.35$. The maxima of $S(\mathbf{k})$ occur at six wave vectors with magnitude $4\pi/(3a)$ (Fig. 9).

As κ is increased, the excitation energy $\omega(\mathbf{k})$ vanishes at some $\mathbf{k}$ values at a critical value of κ. For larger values of κ the system will have magnetic LRO; these states are discussed below.

1. Fluctuations

We now examine the structure of the $1/N$ quantum fluctuations about the $N = \infty$ theory. One of the crucial
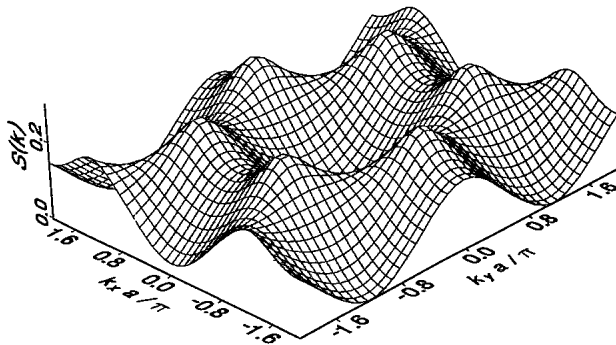

FIG. 9. Zero-temperature structure factor, $S(\mathbf{k})$, of the quantum-disordered ground state of the triangular lattice quantum antiferromagnet. The result is obtained at $N = \infty$, with the "spin" $\kappa = 0.25$. The global maxima are at six wave vectors with magnitude $4\pi/(3a)$. $S(\mathbf{k})$ is computed from Eqs. (2.17) and (2.18).

questions will be the fate of the spin-$\frac{1}{2}$ bosonic spinon excitations that were found above. The main result will be that these excitations remain unconfined for all values of the underlying spin n_b. A previous mechanism for the appearance of spin-Peierls order[28] is ineffective here.

As in previous analyses,[3,4,27,28] it is necessary to study the dynamics of the gauge-field fluctuations. These fields are associated with the compact U(1), lattice gauge symmetry of the action. In particular all physical results are invariant under the transformations

$$b_i^\alpha \to b_i^\alpha \exp(i\rho_i) , \quad Q_{ij} \to Q_{ij} \exp[i(\rho_i + \rho_j)] .$$
(3.6)

The ρ_i is an arbitrary real lattice field generating the U(1) gauge symmetry. For simplicity we have focused on time-independent gauge transformations; time dependence can be included and does not lead to any new structure.[3,4]

After integrating out the b quanta the resulting effective action will be expressed in terms of the deviations of Q_{ij} and λ_i from their mean-field values. The gauge fields arise from the phases of the Q_{ij};[28] we will therefore ignore other fluctuations and parametrize:

$$Q_{i,i+\hat{e}_p} = \bar{Q}_{i,i+\hat{e}_p} \exp(i\Theta_p) ,$$
(3.7)

where $p = 1, 2, 3$, the vectors $\hat{e}_p$ were defined in Eq. (3.3), $\bar{Q}$ is the mean-field value, and Θ_p is a real phase. The effective action for the Θ_p must be invariant under

$$\Theta_p \to \Theta_p + \rho_i + \rho_{i+\hat{e}_p} .$$
(3.8)

Upon performing a Fourier transform, with the link variables Θ_p places on the center of the links, the gauge invariance takes the form

$$\Theta_p(\mathbf{k}) \to \Theta_p(\mathbf{k}) + 2\rho(\mathbf{k}) \cos(k_p/2) .$$
(3.9)

The momentum $\mathbf{k}$ takes values in the first Brillouin zone of the triangular lattice. This invariance implies that the effective action for the Θ_p can only be a function of the following gauge-invariant combinations:

$$I_{pq} = 2\cos(k_q/2)\Theta_p(\mathbf{k}) - 2\cos(k_p/2)\Theta_q(\mathbf{k}) . \quad (3.10)$$

We now wish to take the continuum limit at points in the Brillouin zone where the action involves only gradients of the Θ_p fields and thus has the possibility of gapless excitations. However it is not difficult to see that only two of the three values of $\cos(k_p/2)$ can vanish at any point of the Brillouin zone. One such point is the wave vector

$$\mathbf{g}_a = \frac{2\pi}{\sqrt{3}a}(0,1) ,$$
(3.11)

where

$$g_{a1} = \pi , \quad g_{a2} = -\pi , \quad g_{a3} = 0 .$$
(3.12)

Taking the continuum limit with the fields varying with momenta with close to $\mathbf{g}_a$ we find that the I_{pq} depend only upon gradients of Θ_1 and Θ_2. Under gauge transformations near the momentum $\mathbf{g}_a$, the bosons b_i^α carry

charges $\exp(i\mathbf{g}_a \cdot \mathbf{r}_i)$. It can be verified that these charges only take the values ± 1 on the lattice sites. We have therefore imposed a certain "staggering" of the charge assignments of the bosons which is quite analogous to that in the square-lattice antiferromagnets.[3,4] It is also helpful to parametrize the Θ_p in the following suggestive manner:

$$\begin{aligned}
\Theta_1(\mathbf{r}) &= i A_{a1}(\mathbf{r}) e^{i\mathbf{g}_a \cdot \mathbf{r}} , \\
\Theta_2(\mathbf{r}) &= -i A_{a2}(\mathbf{r}) e^{i\mathbf{g}_a \cdot \mathbf{r}} , \\
\Theta_3(\mathbf{r}) &= \Phi_a(\mathbf{r}) e^{i\mathbf{g}_a \cdot \mathbf{r}} .
\end{aligned} \qquad (3.13)$$

It can be verified that the condition for the reality of Θ_p is equivalent to demanding that A_{a1}, A_{a2}, Φ_a be real. We will now take the continuum limit with A_{a1}, A_{a2}, Φ_a varying slowly on the scale of the lattice spacing. It is then not difficult to show that the invariants I_{pq} then reduce to (after a Fourier transformation)

$$\begin{aligned}
I_{12} &= \hat{\mathbf{e}}_2 \cdot \nabla A_{a1} - \hat{\mathbf{e}}_1 \cdot \nabla A_{a2} , \\
I_{31} &= \hat{\mathbf{e}}_1 \cdot \nabla \Phi_a - 2A_{a1} , \\
I_{32} &= \hat{\mathbf{e}}_2 \cdot \nabla \Phi_a - 2A_{a2} .
\end{aligned} \qquad (3.14)$$

Thus the A_{a1}, A_{a2} are the components of the connection of a gauge symmetry denoted $U_a(1)$; the components are taken along an "oblique" coordinate system defined by the axes $\hat{\mathbf{e}}_1, \hat{\mathbf{e}}_2$. The field Φ_a transforms as the phase of a charge-2 Higgs field under $U_a(1)$.

A very similar analysis can be carried out near the two other points in the Brillouin zone where the other pairs of values of $\cos(k_p/2)$ vanish. These are the points

$$\mathbf{g}_b = \frac{2\pi}{\sqrt{3}a}\left(\frac{\sqrt{3}}{2}, -\frac{1}{2}\right) , \quad \mathbf{g}_c = \frac{2\pi}{\sqrt{3}a}\left(\frac{-\sqrt{3}}{2}, -\frac{1}{2}\right) , \qquad (3.15)$$

which introduce the continuum symmetries $U_b(1)$ and $U_c(1)$, respectively. The Θ_p now reduce in the continuum limit to fields Φ_b, A_{b2}, A_{b3}, and A_{c1}, Φ_c, A_{c3}, respectively. Thus in the continuum limit the lattice U(1) gauge symmetry has been replaced by a $U_a(1) \times U_b(1) \times U_c(1)$ gauge symmetry. The three gauge symmetries correspond to the three different ways the triangular lattice can be distorted into a rectangular lattice with diagonal bonds: the phases on the horizontal and vertical bonds behave like gauge connections while the phases on the diagonal bonds become charge-2 Higgs fields. The system also possesses spin-$\frac{1}{2}$ Bose excitations which carry charges ± 1 of all three symmetries.

The condensation of all of the Higgs fields is implicit, and there are therefore no low-lying physical gauge excitations. Following the reasoning of Refs. 3 and 4 we conclude that the instantons[28] are quenched and that unit charges are expected to be unconfined;[30] in particular the spin-$\frac{1}{2}$ Bose quanta, which carry the $U_a(1)$ charges $\exp(i\mathbf{g}_a \cdot \mathbf{r}_i)$, and analogous $U_b(1)$ and $U_c(1)$ charges, will remain unconfined. The quenching of the instantons also rules out a previous mechanism for the appearance of spin-Peierls order.[28] This can be viewed as another example of the result of Refs. 3 and 4 that spin-Peierls ordering is necessarily induced only in models which have

a magnetically ordered phase with collinear spins; the magnetically ordered phase for the triangular lattice is studied below and will be shown to have noncollinear spins.

B. Magnetically ordered ground state

As was noted in Sec. II, this phase occurs at larger values of κ and the bosonic eigenmodes have at least one zero eigenvalue. Moreover, the condensates x_i^σ must be linear combinations of the eigenvectors associated with this zero mode. The condensate appears for $\kappa > 0.34$ and its energy is shown in Table I as a function of κ. The structure of the condensate can be determined by examining the zero eigenmodes of $\tau^3 D$. The zero eigenvalues of $\tau^3 D$ are at $\mathbf{k} = \tilde{\mathbf{k}}_1$ and $\mathbf{k} = \tilde{\mathbf{k}}_2 = -\tilde{\mathbf{k}}_1$. The existence of these zero modes, or equivalently the stationarity condition (2.16), fixes

$$\lambda = 3\sqrt{3}JQ/2 . \qquad (3.16)$$

The condensate is an arbitrary linear combination of the two zero eigenvectors of $\tau^3 T$: this introduces two complex numbers c_1, c_2, with only the value of $|c_1|^2 + |c_2|^2$ fixed by the saddle-point equations. The final result for the condensate can be easily shown to be

$$\begin{pmatrix} x^\uparrow \\ x^\downarrow \end{pmatrix} = \begin{pmatrix} c_1 & ic_2 \\ ic_2^* & c_1^* \end{pmatrix} \begin{pmatrix} e^{i\mathbf{k}_1 \cdot \mathbf{r}} \\ -i e^{-i\mathbf{k}_1 \cdot \mathbf{r}} \end{pmatrix} . \qquad (3.17)$$

The 2×2 matrix formed by the c_1, c_2 is an SU(2) matrix and performs global spin rotations. Up to such rotations, the condensate is therefore given by the spinors on the rhs of Eq. (3.17). Working out the spin orientations we find that it is of the form of the familiar classical ground state shown in Fig. 10.

The magnitude of the staggered moment $\mathcal{M}$ can be computed by examining the difference between n_b and the value of $\langle b_{i\alpha}^\dagger b_i^\alpha \rangle$ from quantum fluctuations; we find

$$\frac{\mathcal{M}}{N\kappa} = 1 + \frac{1}{\kappa} - \frac{1}{N_s\kappa} \sum_{\mathbf{k}} \frac{\lambda}{\omega(\mathbf{k})} + \mathcal{O}\left(\frac{1}{N}\right) . \qquad (3.18)$$

The constraint (3.16) leads to a cancellation in the dependence of the sum over $\mathbf{k}$ upon Q which is therefore also independent of κ. The sum over $\mathbf{k}$ is a pure number and we find

$$\frac{\mathcal{M}}{N\kappa} = 1 - \frac{0.34}{\kappa} + \mathcal{O}\left(\frac{1}{N}\right) . \qquad (3.19)$$
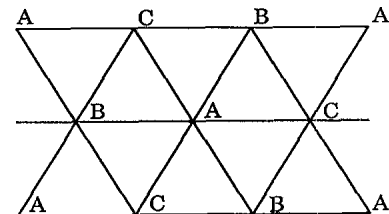

FIG. 10. Spontaneous magnetization of the ground state of the triangular lattice.

IV. KAGOMÉ LATTICE QUANTUM ANTIFERROMAGNET

In this section we will finally apply the formalism developed in Sec. II to the nearest-neighbor quantum Heisenberg antiferromagnet at $T = 0$ on the kagomé lattice. The procedure will be very similar to that of Sec. III.

A. Quantum-disordered phases

Our experience with other lattices[3,4,11] suggests that configurations in which the Q_{ij} and λ_i on every site are equivalent, will include the global minimum of E_{MF}. We will therefore directly specialize to such states. Some of our calculations in subsequent sections will involve much larger unit cells, and will provide independent confirmation of our assertion that allowing inequivalent configurations at the sites does not lower the energy.

Simple considerations show that having chosen $\lambda_i = \lambda$ independent of i, there are only two independent values of Q_{ij}, which are labeled Q_1, Q_2 in Fig. 11. The kagomé lattice with nearest-neighbor spacing a has three sites, u, v, w (Fig. 11), per unit cell of the triangular Bravais lattice with spacing $2a$. We may therefore introduce Fourier-transformed Bose operators $b^\dagger_{u\alpha}(\mathbf{k})$, $b^\dagger_{v\alpha}(\mathbf{k})$, and $b^\dagger_{w\alpha}(\mathbf{k})$ where the momentum $\mathbf{k}$ ranges over the first Brillouin zone of the triangular lattice. We now introduce the operator

$$
\Psi_m(\mathbf{k}) = \begin{pmatrix} b^{m\dagger}_u(\mathbf{k}) \\ b^{m\dagger}_v(\mathbf{k}) \\ b^{m\dagger}_w(\mathbf{k}) \\ b^\dagger_{um\downarrow}(-\mathbf{k}) \\ b^\dagger_{vm\downarrow}(-\mathbf{k}) \\ b^\dagger_{wm\downarrow}(-\mathbf{k}) \end{pmatrix} .
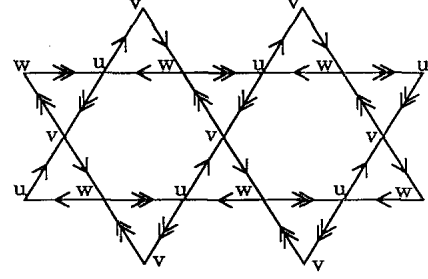\tag{4.1}
$$

FIG. 11. Configurations of the Q_{ij} chosen on the kagomé lattice with nearest-neighbor spacing a. We allow for only two independent link variables Q_1, Q_2; the links with single arrows have $Q_{ij} = Q_1$, while the links with double arrows have $Q_{ij} = Q_2$. The $\lambda_i = \lambda$ on all sites. Also shown are three sites u, v, w which form the unit cell of the triangular Bravais lattice with spacing $2a$.

The index $m = 1, \ldots, N$ and will not be explicitly displayed any more. Its chief role is to provide a prefactor N when the bosons are integrated out. The mean-field Hamiltonian now takes the form

$$
\frac{H_{\mathrm{MF}}}{NN_s} = \frac{1}{N_s} \sum_{\mathbf{k}} \Psi^\dagger(\mathbf{k}) D(\mathbf{k}) \Psi(\mathbf{k})
$$
$$
+ \frac{J}{2}(|Q_1|^2 + |Q_2|^2) - \lambda(1 + \kappa) ,
\tag{4.2}
$$

where the 6×6 matrix $D(\mathbf{k})$ has the form

$$
D(\mathbf{k}) = \begin{pmatrix} \lambda \mathbb{1} & P(\mathbf{k}) \\ P^\dagger(\mathbf{k}) & \lambda \mathbb{1} \end{pmatrix}
\tag{4.3}
$$

with $\mathbb{1}$ the 3×3 unit matrix and P given by

$$
P(\mathbf{k}) = \frac{J}{2} \begin{pmatrix} 0 & Q_1 e^{-ik_1} + Q_2 e^{ik_1} & -Q_1 e^{ik_3} - Q_2 e^{-ik_3} \\ -Q_1 e^{ik_1} - Q_2 e^{-ik_1} & 0 & Q_1 e^{-ik_2} + Q_2 e^{ik_2} \\ Q_1 e^{-ik_3} + Q_2 e^{ik_3} & -Q_1 e^{ik_2} - Q_2 e^{-ik_2} & 0 \end{pmatrix} .
\tag{4.4}
$$

The k_p were defined in Eqs. (3.2) and (3.3).

To determine the eigenmodes of H_{MF} we need to diagonalize $\tau^3 D$. For the special case where λ_i are independent of i, the problem can be further simplified. It is not difficult to show that the eigenvalues $[\omega_\mu(\mathbf{k}), -\omega_\mu(\mathbf{k})]$ of $\tau^3 D$ can be expressed in terms of the eigenvalues of $P^\dagger P$. In particular, with

$$
P^\dagger(\mathbf{k}) P(\mathbf{k}) \varphi_\mu(\mathbf{k}) = p^2_\mu(\mathbf{k}) \varphi_\mu(\mathbf{k}) ,
\tag{4.5}
$$

where p^2_μ, $\mu = 1, 2, 3$ are the eigenvalues and $\varphi_\mu(\mathbf{k})$ the eigenvectors, we find

$$
\omega_\mu(\mathbf{k}) = [\lambda^2 - p^2_\mu(\mathbf{k})]^{1/2} .
\tag{4.6}
$$

Finally the ground-state energy can be determined to be

$$
\frac{E_{\mathrm{MF}}}{NN_s} = \frac{1}{N_s} \sum_{\mathbf{k}, \mu} \omega_\mu(\mathbf{k}) + \frac{J}{2}(|Q_1|^2 + |Q_2|^2) - \lambda(1 + \kappa) .
\tag{4.7}
$$

We numerically minimized E_{MF} with respect to the complex numbers Q_1 and Q_2 subject to the condition (3.5). For values of κ small enough to prevent magnetic LRO (discussed below), two locally stable solutions were found. In a suitable gauge Q_1 and Q_2 could be made real for both solutions, showing that time-reversal symmetry remains unbroken in the quantum disordered phase. The solutions were (a) $Q_1 = -Q_2$ and (b) $Q_1 = Q_2$. These two states are physically distinct and cannot be transformed into one another by gauge transformations. Their

TABLE II. Kagomé-lattice quantum antiferromagnet: mean-field energies for the $Q_1 = Q_2$ and $Q_1 = -Q_2$ states at $T = 0$ as a function of $\kappa = n_B/N$. Tabulated are the values of $E_{MF}/(JNN_s/2)$. The $Q_1 = Q_2$ state has magnetic LRO for $\kappa > 0.50$, while the $Q_1 = -Q_2$ state has magnetic LRO for $\kappa > 0.53$. The $Q_1 = -Q_2$ state is always lower in energy.

κ	$Q_1 = -Q_2$	$Q_1 = Q_2$
0.1	−0.109 04	−0.108 98
0.2	−0.2374	−0.2370
0.3	−0.3871	−0.3860
0.4	−0.560	−0.558
0.5	−0.760	−0.757
0.75	−1.388	−1.384
1.00	−2.203	−2.198
1.25	−3.205	−3.199
1.50	−4.395	−4.389

energies as a function of κ are shown in Table II. Notice that the first solution $Q_1 = -Q_2$ is always the lower in energy for all values of κ, including those with long-range magnetic order.

We also have available in $\omega_\mu(\mathbf{k})$ the excitation spectrum of these states. We show in Figs. 4 and 12 the momentum dependence of the energy of the lowest excited spinon state at $\kappa = 0.35$. Notice first that both states have a finite energy gap at this value of κ. The minimum energy excitations of the $Q_1 = -Q_2$ ground state are the spinons at $\mathbf{k} = \mathbf{k}_1 = (2\pi/3a)(1,0)$ and $\mathbf{k} = \mathbf{k}_2 = (2\pi/3a)(-1,0)$ and other points separated from $\mathbf{k}_1, \mathbf{k}_2$ by vectors of the reciprocal lattice generated by $\mathbf{G}_1 = (2\pi/\sqrt{3}a)(0,1)$ and $\mathbf{G}_2 = (2\pi/\sqrt{3}a)(\sqrt{3}/2,-1/2)$. The minimum excitations above the ground state $Q_1 = Q_2$ is the spinon at $\mathbf{k} = 0$ and other points separated from it by vectors of the reciprocal lattice. The spin structure factor, $S(\mathbf{k})$ of both states was computed using Eq. (2.20): the results are shown in Figs. 5 and 13 for the quan-
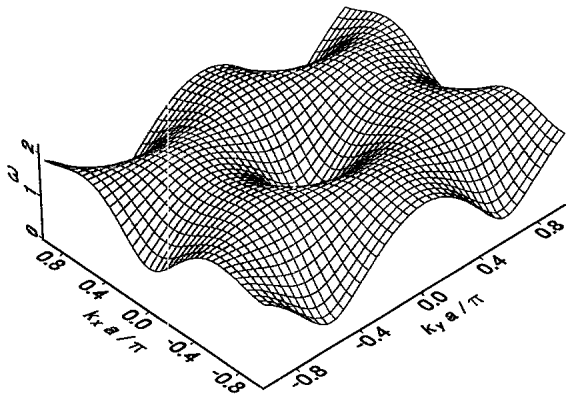

FIG. 12. Momentum dependence of the energy, $\omega(\mathbf{k})$ of the lowest excited spinon state of the kagomé-lattice quantum antiferromagnet for the $Q_1 = Q_2$ state at $\kappa = 0.35$. The minimum excitation energy is the spinon at $\mathbf{k} = 0$ and other points separated from it by vectors of the reciprocal lattice generated by $\mathbf{G}_1 = (2\pi/\sqrt{3}a)(0,1)$ and $\mathbf{G}_2 = (2\pi/\sqrt{3}a)(\sqrt{3}/2,-1/2)$.
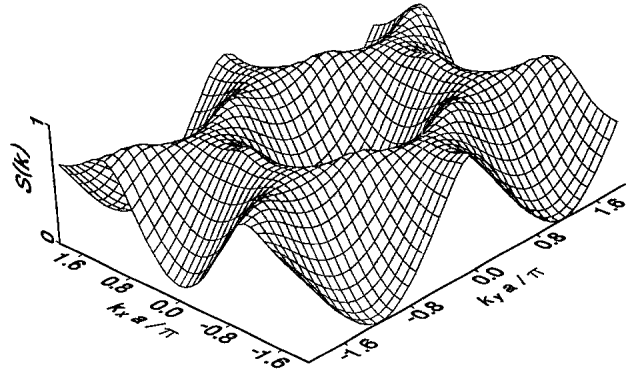

FIG. 13. Zero-temperature structure factor, $S(\mathbf{k})$, for the $Q_1 = Q_2$ state of the kagomé-lattice quantum antiferromagnet at $\kappa = 0.35$. $S(\mathbf{k})$ is computed from Eqs. (2.17) and (2.18), and has local maxima at six wave vectors with magnitude $4\pi/(3a)$. Notice however the ridges going into, e.g., $(0, 2\pi/a)$; the true maxima in fact occur at $(0, 2\pi/a)$ and points related to it by symmetry.

tum disordered states at $\kappa = 0.35$. The maxima of $S(\mathbf{k})$ for the $Q_1 = -Q_2$ ground state occur at six wave vectors with magnitude $4\pi/(3a)$ (Fig. 5). The metastable $Q_1 = Q_2$ state also has local maxima at $4\pi/(3a)$. Notice however the ridges in Fig. 13 going into, e.g., $(2\pi/a, 0)$; the true maxima in fact occur at $(2\pi/a, 0)$ and points related to it by symmetry. These ridges may therefore serve as an experimentally distinguishing feature of the two states. The ridges will probably by wiped out in a powder average: it is therefore necessary to study single-crystal samples. Further information on the nature of the spin correlations in the two states will appear when we discuss the associated phases with magnetic LRO below.

1. Fluctuations

The analysis of the $1/N$ fluctuations about the above quantum disordered states closely follows parallels that of Sec. III A 1 for the triangular lattice. There are additional complications due to the presence of a larger number of sites in the unit cell, but the essential features will be shown to remain unchanged. Thus we will find that the lattice U(1) gauge symmetry is replaced in the continuum limit by a $U_a(1) \times U_b(1) \times U_c(1)$ gauge symmetry; condensation of charge-2 Higgs fields will quench the gauge forces and the spin-$\frac{1}{2}$ spinon excitations will remain unconfined. Spin-Peierls order is also not expected to appear.
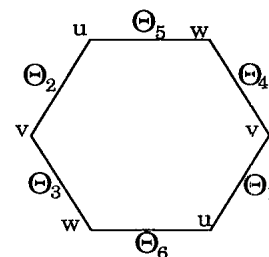

FIG. 14. Labeling of the three sublattices u, v, w and the six links of a unit cell of the kagomé lattice for Sec. IV A 1.

The kagomé lattice has three sites, and therefore six links per unit cell. We number the links as shown in Fig. 14, and leading to six phase variables Θ_{1-6} associated with the phases of the Q_{ij} [see Eq. (3.7)]. It is also necessary to have three fields ρ_u, ρ_v, ρ_w which generate gauge transformations. After a Fourier transform, the effective action for the Θ_p must be invariant under the transformations (this is the analog of Eq. [3.9]):

$$\Theta_1 \rightarrow \Theta_1 + \rho_u e^{-ik_1/2} + \rho_v e^{ik_1/2} ,$$
$$\Theta_2 \rightarrow \Theta_2 + \rho_u e^{ik_1/2} + \rho_v e^{-ik_1/2} ,$$
$$\Theta_3 \rightarrow \Theta_3 + \rho_v e^{-ik_2/2} + \rho_w e^{ik_2/2} ,$$

$$(4.8)$$

$$\Theta_4 \rightarrow \Theta_4 + \rho_v e^{ik_2/2} + \rho_w e^{-ik_2/2} ,$$
$$\Theta_5 \rightarrow \Theta_5 + \rho_w e^{-ik_3/2} + \rho_u e^{ik_3/2} ,$$
$$\Theta_6 \rightarrow \Theta_6 + \rho_w e^{ik_3/2} + \rho_u e^{-ik_3/2} .$$

A little experimentation shows that the structure of these equations becomes evident upon the following decomposition of the field generating the gauge transformations

$$\rho_u = \rho_b + \rho_c - \rho_a , \quad \rho_v = \rho_c + \rho_a - \rho_b , \quad \rho_w = \rho_a + \rho_b - \rho_c .$$

$$(4.9)$$

The fields ρ_a, ρ_b, ρ_c will be shown below to generate the $U_a(1), U_b(1), U_c(1)$ gauge transformations in the continuum limit. From Eq. (4.9) we therefore deduce that the bosons on the u, v, w sublattices carry charges $-1, +1, +1$ under $U_a(1)$, $+1, -1, +1$ under $U_b(1)$, and $+1, +1, -1$ under $U_c(1)$. Inserting (4.9) in (4.8) we obtain

$$\Theta_1 \rightarrow \Theta_1 + 2\rho_c \cos(k_1/2) - 2i(\rho_b - \rho_a)\sin(k_1/2) ,$$
$$\Theta_2 \rightarrow \Theta_2 + 2\rho_c \cos(k_1/2) + 2i(\rho_b - \rho_a)\sin(k_1/2) ,$$
$$\Theta_3 \rightarrow \Theta_3 + 2\rho_a \cos(k_2/2) - 2i(\rho_c - \rho_b)\sin(k_2/2) ,$$

$$(4.10)$$

$$\Theta_4 \rightarrow \Theta_4 + 2\rho_a \cos(k_2/2) + 2i(\rho_c - \rho_b)\sin(k_2/2) ,$$
$$\Theta_5 \rightarrow \Theta_5 + 2\rho_b \cos(k_3/2) - 2i(\rho_a - \rho_c)\sin(k_3/2) ,$$
$$\Theta_6 \rightarrow \Theta_6 + 2\rho_b \cos(k_3/2) + 2i(\rho_a - \rho_c)\sin(k_3/2) .$$

The unit cell of the kagomé lattice is large enough that the continuum limit can be taken at $\mathbf{k} = 0$. We therefore introduce the decompositions

$$\Theta_1 = \Phi_c + A_{b1} - A_{a1} , \quad \Theta_2 = \Phi_c - A_{b1} + A_{a1} ,$$
$$\Theta_3 = \Phi_a + A_{c2} - A_{b2} , \quad \Theta_4 = \Phi_a - A_{c2} + A_{b2} , \quad (4.11)$$
$$\Theta_5 = \Phi_b + A_{a3} - A_{c3} , \quad \Theta_6 = \Phi_b - A_{a3} + A_{c3} ,$$

where all the fields on the rhs are assumed to be slowly varying on the scale of the lattice spacing. From these decompositions and the continuum limit of Eq. (4.10) we obtain the fields associated with $U_a(1)$

$$A_{a1} \rightarrow A_{a1} - \hat{\mathbf{e}}_1 \cdot \nabla\rho_a , \quad A_{a3} \rightarrow A_{a3} - \hat{\mathbf{e}}_3 \cdot \nabla\rho_a ,$$
$$\Phi_a \rightarrow \Phi_a - 2\rho_a, \quad (4.12a)$$

with $U_b(1)$

$$A_{b2} \rightarrow A_{b2} - \hat{\mathbf{e}}_2 \cdot \nabla\rho_b , \quad A_{b1} \rightarrow A_{b1} - \hat{\mathbf{e}}_1 \cdot \nabla\rho_b ,$$
$$\Phi_b \rightarrow \Phi_b - 2\rho_b , \quad (4.12b)$$

and with $U_c(1)$

$$A_{c3} \rightarrow A_{c3} - \hat{\mathbf{e}}_3 \cdot \nabla\rho_c , \quad A_{c2} \rightarrow A_{c2} - \hat{\mathbf{e}}_2 \cdot \nabla\rho_c ,$$
$$\Phi_c \rightarrow \Phi_c - 2\rho_c . \quad (4.12c)$$

We have thus obtained connections and phases of charge-2 Higgs fields for $U_a(1)$, $U_b(1)$, and $U_c(1)$. The dynamics of the gauge fields must be controlled by an action which is invariant under the above transformations.

The subsequent reasoning is identical to that at the end of Sec. III A 1 and leads to the same conclusions. The spinons are liberated by the condensation of the charge-2 Higgs scalars and spin-Peierls order is not expected to appear.

B. Magnetically ordered phases

We will consider the LRO phases associated with the two SRO phases in turn.

1. $Q_1 = -Q_2$

The condensate appears for $\kappa > 0.53$. The energy of this state is shown in Table II as a function of κ. The structure of the condensate can be determined by examining the zero eigenmodes of $\tau^3 D$. The zero eigenvalues of $\tau^3 D$ are at $\mathbf{k} = \mathbf{k}_1$ and $\mathbf{k} = \mathbf{k}_2 = -\mathbf{k}_1$, which were defined in Sec. IV A. The existence of these zero modes now fixes

$$\lambda = \sqrt{3}J|Q_1| . \quad (4.13)$$

Both eigenvalues are nondegenerate and the associated eigenvectors are

$$\Psi_1 = (i, -i, i, 1, -1, 1)e^{i\mathbf{k}_1 \cdot \mathbf{r}} ,$$

$$(4.14)$$

$$\Psi_2 = (-i, i, -i, 1, -1, 1)e^{-i\mathbf{k}_1 \cdot \mathbf{r}} .$$

We take a condensate of the form $c_1\Psi_1 + c_2\Psi_2$, where only $|c_1|^2 + |c_2|^2$ will be determined by the saddle-point conditions. Working out the orientation of the condensate at every lattice site we find that it can be written in the form

$$\begin{pmatrix} x_u^\uparrow \\ x_u^\downarrow \end{pmatrix} = \begin{pmatrix} c_1 & -ic_2 \\ -ic_2^* & c_1^* \end{pmatrix} \begin{pmatrix} ie^{i\mathbf{k}_1 \cdot \mathbf{r}} \\ e^{-i\mathbf{k}_1 \cdot \mathbf{r}} \end{pmatrix} ,$$

$$\begin{pmatrix} x_v^\uparrow \\ x_v^\downarrow \end{pmatrix} = -\begin{pmatrix} c_1 & -ic_2 \\ -ic_2^* & c_1^* \end{pmatrix} \begin{pmatrix} ie^{i\mathbf{k}_1 \cdot \mathbf{r}} \\ e^{-i\mathbf{k}_1 \cdot \mathbf{r}} \end{pmatrix} , \quad (4.15)$$

$$\begin{pmatrix} x_w^\uparrow \\ x_w^\downarrow \end{pmatrix} = \begin{pmatrix} c_1 & -ic_2 \\ -ic_2^* & c_1^* \end{pmatrix} \begin{pmatrix} ie^{i\mathbf{k}_1 \cdot \mathbf{r}} \\ e^{-i\mathbf{k}_1 \cdot \mathbf{r}} \end{pmatrix} .$$

The 2×2 matrix formed by the c_1, c_2 is again an SU(2) matrix and performs global spin rotations. Working out the spin orientations we find that it is of the form shown in Fig. 2. The spin arrangement forms a triangular lattice with a $\sqrt{3} \times \sqrt{3}$ unit cell of 9 sites. Moreover, suitably oriented spins can be added to the center of every hexagon to yield the ground state of the antiferromagnet on a triangular lattice of spacing a.

The magnitude of the staggered moment $\mathcal{M}$ is computed as in Sec. III B to be

$$\frac{\mathcal{M}}{N\kappa} = 1 - \frac{0.53}{\kappa} + \mathcal{O}\left(\frac{1}{N}\right) . \qquad (4.16)$$

The $1/N$ fluctuations of this state will involve consideration of the fluctuations in Q_{ij}, λ_i, and x_i^g. Note that because $\tilde{b}$ bosons were integrated over, order-by-disorder effects are already included in the saddle point. Thus the propagators of the x_i^g will only carry zero energy at $k = 0$ and there will be no modes which are zero at all wave vectors (such modes occur in the semiclassical expansion[16,18]). It is only in the limit $\kappa = \infty$ that the propagators become singular over the entire Brillouin zone. We will explicitly demonstrate the nonsingular nature of the x_i^g propagators by examining the energy associated with space-dependent deformations of the x_i^g in Sec. V.

2. $Q_1 = Q_2$

The condensate appears for $\kappa > 0.50$. The energy is shown in Table II and is higher than that of the $Q_1 = -Q_2$ state. The zero eigenvalue of $\tau^3 D$ is at $k = 0$. The condition (2.16) leads again to the restriction (4.13) on the value of λ. The zero mode is found to be doubly degenerate. The two eigenvectors are

$$\Psi_1 = (1, 1, -2, \sqrt{3}, -\sqrt{3}, 0) ,$$

$$\qquad (4.17)$$

$$\Psi_2 = (-\sqrt{3}, \sqrt{3}, 0, 1, 1, -2) .$$

The condensate is therefore of the form $c_1\Psi_1 + c_2\Psi_2$, where only $|c_1|^2 + |c_2|^2$ will be determined by the saddle-point equations. Working out the orientation of the condensate at every lattice site, we find that it can be written in the form

$$\begin{pmatrix} x_u^\uparrow \\ x_u^\downarrow \end{pmatrix} = \begin{pmatrix} c_1 & -c_2 \\ c_2^* & c_1^* \end{pmatrix} \begin{pmatrix} 1 \\ \sqrt{3} \end{pmatrix} ,$$

$$\begin{pmatrix} x_v^\uparrow \\ x_v^\downarrow \end{pmatrix} = \begin{pmatrix} c_1 & -c_2 \\ c_2^* & c_1^* \end{pmatrix} \begin{pmatrix} 1 \\ -\sqrt{3} \end{pmatrix} , \qquad (4.18)$$

$$\begin{pmatrix} x_w^\uparrow \\ x_w^\downarrow \end{pmatrix} = \begin{pmatrix} c_1 & -c_2 \\ c_2^* & c_1^* \end{pmatrix} \begin{pmatrix} -2 \\ 0 \end{pmatrix} .$$

Up to global rotations the spin orientations are of the form shown in Fig. 3, where A, B, C are spins pointing toward the vertices of an equilateral triangle (Fig. 1). The unit cell of the spin arrangement is the same as the unit cell of the lattice and this is therefore a $k = 0$ state.

The magnitude of the staggered moment can be computed as above to yield

$$\frac{\mathcal{M}}{N\kappa} = 1 - \frac{0.50}{\kappa} + \mathcal{O}\left(\frac{1}{N}\right) . \qquad (4.19)$$

V. ORDERING BY QUANTUM FLUCTUATIONS

A limitation of the kagomé lattice mean-field analysis of Sec. IV is that the energy was minimized over a rather limited set of variational parameters. The parameters were certainly not general enough to explore the large

space of degenerate ground states that appear in the classical limit. A complete self-consistent mean-field analysis which does this would be computationally prohibitive. However, substantial progress can be made in the large-κ limit discussed in Sec. II B; we shall find that physics of ordering by quantum fluctuations becomes especially clear in this limit. The basic procedure we shall follow is this: choose any one of the classical ground states of the kagomé lattice and compute the first quantum correction E_1 [Eqs. (2.21) and (2.25)] to its energy. We shall provide a convincing demonstration in this section that the quantum fluctuations lift the degeneracy between the classical ground states down to that associated with a single, uniform, global rotation of the spins. The true quantum ground state on the kagomé lattice will continue to be the $Q_1 = -Q_2$ state of Sec. IV and Fig. 2. All of the analysis in this section refers implicitly to the kagomé-lattice quantum Heisenberg antiferromagnet at $T = 0$.

We shall study the lifting of the classical degeneracy in two steps. We will begin in Sec. V A by considering all the classical ground states in which the spins are coplanar. The spins will therefore be restricted to point in the three directions A, B, C (Fig. 1), with no two nearest-neighbor pairs having the same orientation. Quantum fluctuations will select a particular arrangement of the spins. Then in Sec. V B we will consider classical ground states with noncoplanar spins; quantum fluctuations will raise their energy over the coplanar states for the infinite lattice.

A. Coplanar spins

Restricting the spins to point in one of the three coplanar directions A, B, C (Fig. 1) still leaves the classical kagomé Heisenberg antiferromagnet with a finite ground-state entropy. Any state in which no two nearest neighbors have the same orientation is a classical ground state. The number of such states increases exponentially with the system size, and are in one-to-one correspondence with the ground states of the 3-state Potts antiferromagnet on the kagomé lattice.

We will restrict our attention to the infinite-lattice classical states which are periodic with the 27-site unit cell shown in Fig. 15. A simple calculation shows that there are a total of 120 distinct coplanar states which have this periodicity. Three of these states are shown in Fig. 15. The state in Fig. 15(a) was asserted to be the ground state in Sec. IV B.

We have computed the first quantum correction, E_1 [Eq. (2.21)] for all the 120 classical states described above. Each classical spin orientation determines the x_i^{gc} up to a gauge transformation. We then determined Q_{ij}^c, λ_i^c for each classical spin orientation from Eqs. (2.22) and (2.23) and found

$$Q_{ij}^c = \pm\sqrt{3}\kappa/2 , \quad \lambda_i^c = 3\kappa J/2 . \qquad (5.1)$$

All of the information on the location of the A, B, C spins is carried in the sign of the Q_{ij}. The eigenenergies were determined by solving Eq. (2.12), and E_1 evaluated from Eq. (2.25).

The values of E_1 for the states in Fig. 15 were

$$\frac{E_1}{N_s J \kappa / 2} = \begin{cases} -0.635\,324 & \text{Fig. 15(a)} \\ -0.631\,406 & \text{Fig. 15(b)} \\ -0.633\,958 & \text{Fig. 15(c)}. \end{cases} \qquad (5.2)$$
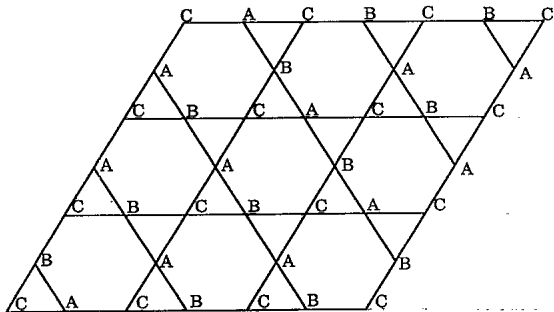
The state in Fig. 15(a), and 5 others related to it by lattice symmetries, were found to have the lowest energy. The values of E_1 of all other 115 states were higher, with the highest energy being carried by the state in Fig. 15(b) and its 5 symmetry-related partners.
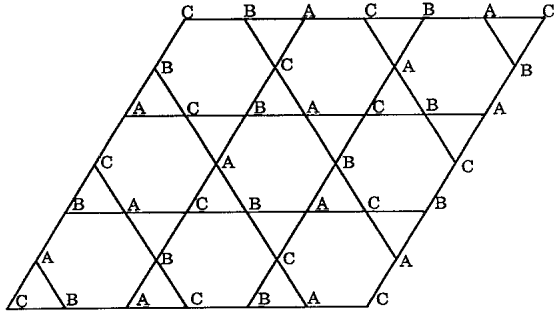
(a)
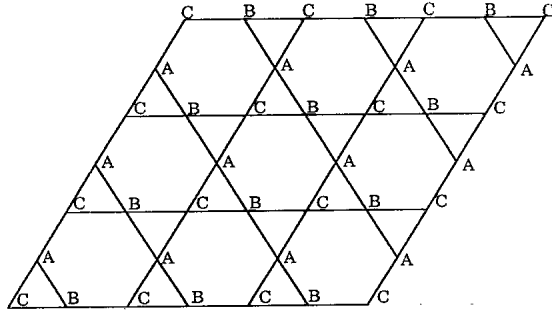
(b)

(c)

FIG. 15. Coplanar spin arrangements which are periodic with the shown 27-site unit cells. There are 120 such arrangements of which 3 are shown. The configuration in (a) is found to have the lowest quantum-corrected energy, while that in (b) has the highest.

Quantum fluctuations have therefore been shown to induce order among the manifold of ground states of the classical 3-state Potts antiferromagnet. The states selected have the ordering of Fig. 2 with a $\sqrt{3} \times \sqrt{3}$ unit cell of 9 sites.

B. Noncoplanar spins

Consider the planar state selected in Sec. V A. If we allow for noncoplanar spins, this state (and all other classical states) has some remarkable additional classical degeneracies. For example, the B and C spins around a given hexagon can be rotated about the axis defined by the A spin with no change in the classical energy—the angle of rotation can be different on each hexagon of B and C spins. We will show in this subsection that this degeneracy is reduced to a single global rotation once the finite-κ quantum fluctuations have been included. We will compute the quantum correction E_1 for a large number of noncoplanar spin arrangements. The method of the calculation is identical to that described in Sec. V A. The end result will be that quantum fluctuations in the infinite kagomé lattice endow coplanar states with a lower energy.

Let us orient all the A spins in Fig. 2 or Fig. 15(a) along the z axis. The B, C spins around each hexagon define a plane which is perpendicular to the xy plane. Let ϕ be the angle between this plane and the xz plane. Clearly, the angle ϕ can take an arbitrary value in each hexagon of B, C spins in the classical limit. We have therefore

$$\mathbf{S}_A = \kappa(0, 0, 1) \,,$$

$$\mathbf{S}_B = \kappa \left(\frac{\sqrt{3}}{2} \cos \phi, \frac{\sqrt{3}}{2} \sin \phi, -\frac{1}{2} \right) \,, \qquad (5.3)$$

$$\mathbf{S}_C = \kappa \left(-\frac{\sqrt{3}}{2} \cos \phi, -\frac{\sqrt{3}}{2} \sin \phi, -\frac{1}{2} \right) \,.$$

The associated values of the spinor condensates x^c are

$$x_A^c = \sqrt{\kappa} \begin{pmatrix} 1 \\ 0 \end{pmatrix} \quad x_B^c = \sqrt{\kappa} \,, \quad \begin{pmatrix} 1/2 \\ (\sqrt{3}/2) e^{i\phi} \end{pmatrix} \,,$$

$$\qquad (5.4)$$

$$x_C^c = \sqrt{\kappa} \begin{pmatrix} 1/2 \\ -(\sqrt{3}/2) e^{i\phi} \end{pmatrix} \,.$$

The values of the link variables Q_{ij}^c can now be determined from Eq. (2.23). We find

$$Q_{ij}^c = \pm(\sqrt{3}\kappa/2) e^{-i\phi} \,. \qquad (5.5)$$

All of the information on the orientation of the B, C hexagons is carried in the phases of the Q_{ij}^c. The "classical" energy $E_c = -\sum_{i>j} |Q_{ij}^c|^2$ is independent of the ϕ values and therefore of the orientation of the hexagons. Finally, the Lagrange multipliers λ_i^c can be determined by solving Eq. (2.16). The answers again turn out to be independent of the ϕ values. They depend only upon whether i is in the bulk or on the boundary of the various clusters that we consider below:
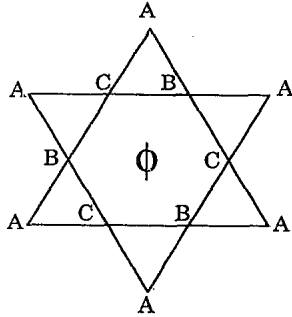
FIG. 16. The 12-site hexagram. The A spins point along the z axis. The plane defined by the B, C spins is perpendicular to the xy plane and makes an angle ϕ with the xz plane.

$$\lambda_i^c = \begin{cases} 3\kappa J/2 & \text{for } i \text{ in the bulk} \\ 3\kappa J/4 & \text{for } i \text{ on the boundary.} \end{cases} \quad (5.6)$$

We now study the manner in which the classical local degeneracy is lifted by the first quantum correction E_1 [Eqs. (2.21) and (2.25)]. We will consider various finite and infinite clusters made out of the basic unit shown in Fig. 16: 12 sites arranged in a "hexagram"; the boundary spins are in the A direction, while the spins around the hexagon are in the B and C directions. There will be an angle ϕ associated with the B, C hexagon in every hexagram. Clearly the energy of a single hexagram is independent of its ϕ, as changes in ϕ are global rotations of spins on the cluster.

We now consider various combinations of the hexagrams.

1. Two hexagrams

These form a 23-site cluster (Fig. 17), with the two hexagrams sharing a common A site. We can use global spin rotation invariance to choose $\phi = 0$ on one hexagram. Let $\phi = \phi_1$ on the second hexagram. We now evaluate E_1 by determining the boson spectrum and then using Eq. (2.25); we find that E_1 is independent of ϕ_1. Evidently the single common site does not lead to quantum interference between motion of the bosons on the two hexagrams. We have verified that the energy remains independent of ϕ_1 to all orders in $1/\kappa$.
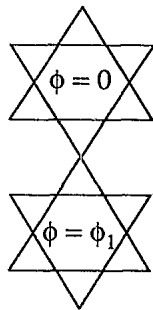

FIG. 17. Two of the hexagrams of Fig. 16 forming a 23-site cluster. The full quantum energy is found to be independent of ϕ_1.
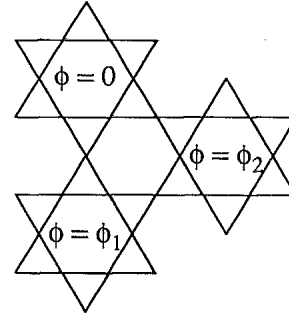

FIG. 18. Three of the hexagrams of Fig. 16 forming a 33-site cluster. The quantum corrections minimize the energy at $\phi_1 = 2\pi/3$ and $\phi_2 = 4\pi/3$. The spin condensates are therefore not coplanar but truly three dimensional.

2. Three hexagrams

This 33-site cluster is shown in Fig. 18. The energy E_1 is now dependent on ϕ_1 and ϕ_2. It is a minimum at $\phi_1 = 2\pi/3$ and $\phi_2 = 4\pi/3$. The optimum spin arrangement of this finite cluster is therefore truly noncoplanar. No part of the infinite lattice ground state in Sec. IV B has such a structure.

3. Seven hexagrams

The 72-site cluster in Fig. 19 is a still larger chunk of the infinite kagomé lattice. The energy E_1 is dependent on all the ϕ's and has its minimum at $\phi_1 = \phi_2 = \phi_3 = \phi_4 = \phi_5 = \phi_6 = 0$. This arrangement is planar and compatible with the infinite-lattice $\sqrt{3} \times \sqrt{3}$ ground state.

4. Three hexagrams: periodic boundary conditions

We consider next the 27-site cluster obtained by identifying opposite edges of the rhombus in Fig. 20. All the sites are equivalent and the cluster retains all the rotational symmetries of the infinite kagomé lattice. The
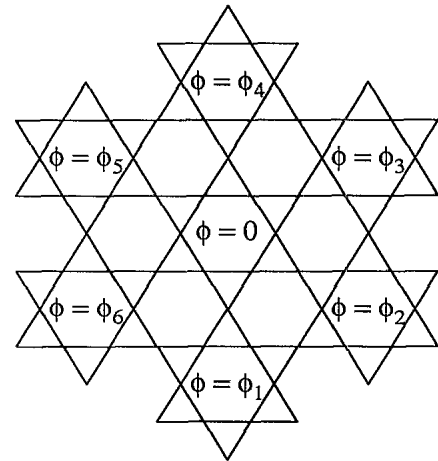

FIG. 19. Seven of the hexagrams of Fig. 16 forming a 72-site cluster. The quantum corrections minimize the energy at $\phi_1 = \phi_2 = \phi_3 = \phi_4 = \phi_5 = \phi_6 = 0$. The spin condensates are therefore coplanar.
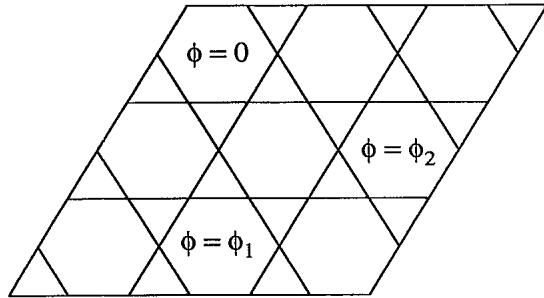
FIG. 20. Identifying the opposite edges of this rhombus yields a 27-site cluster with three hexagrams and the full rotational symmetry of the kagomé lattice; the orientation of the spins around each hexagram is as in Fig. 16. The minimum energy is found at $\phi_1 = 2\pi/3$ and $\phi_2 = 4\pi/3$. We may also treat this cluster as the 27-site unit cell of an infinite lattice. In this case the quantum corrections lower the energy most at $\phi_1 = \phi_2 = 0$.

minimum energy state is found to be the same as that of the three-hexagram configuration with open boundary conditions (Fig. 18): $\phi_1 = 2\pi/3$ and $\phi_2 = 4\pi/3$. The values of $E_1/J\kappa$ as a function of ϕ_1, ϕ_2 are shown in Fig. 21.

5. Three-hexagram unit cell of infinite lattice

Finally, we use the 27-site configuration of Fig. 20 as a unit cell of the infinite kagomé lattice. The x^c condensates are obtained by repeating the arrangement in Fig. 20 periodically: the final configuration forms a triangular lattice with a 27-site unit cell. The bosons are free to move on this infinite lattice and their spectrum differs from that in the cluster in Sec. V B 4. We find that E_1 now has a minimum at $\phi_1 = 0$, $\phi_2 = 0$. The values of $E_1/J\kappa$ as a function of ϕ_1, ϕ_2 are shown in Fig. 22.
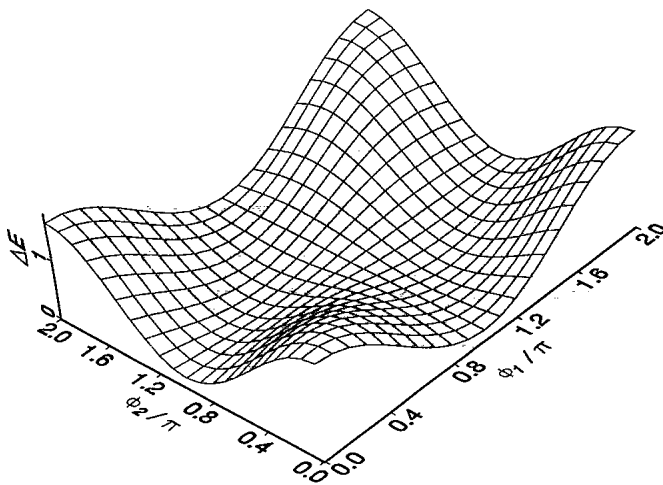

FIG. 21. The first quantum correction to the energy $E_1/J\kappa$ as a function of the angles ϕ_1 and ϕ_2 for the 27-site finite cluster obtained by identifying the opposite edges of the rhombus in Fig. 20 (Sec. V B 4). The vertical axis is $\Delta E_1 = 2 \times 10^3 \times (E_1 - E_{1\min})/(N_s J\kappa)$. We find $E_{1\min}/(N_s J\kappa/2) = -0.673\,943$ at $\phi_1 = 2\pi/3$, $\phi_2 = 4\pi/3$ and vice versa.
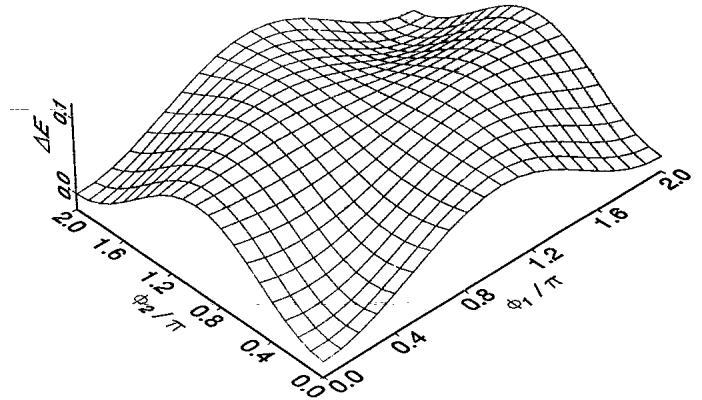

FIG. 22. As in Fig. 21 but for the infinite kagomé lattice with the 27-site rhombus in Fig. 20 treated as a unit cell (Sec. V B 5). We find now $E_{1\min}/(N_s J\kappa/2) = -0.635\,324$ at $\phi_1 = \phi_2 = 0$.

This lowest energy state is therefore fully consistent with the $\sqrt{3} \times \sqrt{3}$ ground state studied in Sec. IV B and provides additional evidence supporting our assertion that the configuration of Fig. 11 with $Q_1 = -Q_2$, or equivalently the ordered state of Fig. 2 or Fig. 15(a), is in fact global minimum of the energy.

6. Discussion

A remarkable feature of the above results is that small clusters with periodic or free boundary conditions actually prefer noncoplanar spin arrangements. It was only when quite large (Sec. V B 3) or infinite lattices (Sec. V B 5) were considered that the planar configurations eventually won out. This suggests that the effective Hamiltonian for the "rotor" variables associated with each B, C hexagon is quite nonlocal and is dominated by many-rotor interactions.

VI. CONCLUSIONS

This paper has presented a systematic large-N analysis of Heisenberg antiferromagnets on the kagomé and triangular lattices. We will recapitulate the main results on zero temperature, quantum-disordered phases in Sec. VI A; this will be followed by a comparison with other theoretical results on such phases. The same will be done for the magnetically ordered phases of the quantum antiferromagnets in Sec. VI B and for the classical antiferromagnet in Sec. VI C. Finally in Sec. VI D we will discuss implications for experiments.

A. Quantum-disordered phases

For small values of the "spin" on each site, the quantum antiferromagnets on both lattices displayed quantum-disordered ground states which are very similar in structure. These ground states do not break any symmetry. They possess a gap and the low-lying excitations are unconfined, bosonic, spin-$\frac{1}{2}$ spinons. These free spin-$\frac{1}{2}$ excitations exist for all values of the on-site

spin. The spinons also carry charges ± 1 of a continuum $U_a(1) \times U_b(1) \times U_c(1)$ gauge symmetry, which is the remnant of a single lattice U(1) internal gauge invariance. All three continuum U(1)'s are in a Higgs phase due to the condensation of charge +2 scalars. This quenches the confinement of unit charges[30] and the spinons remain free. It also disables a previous mechanism for the introduction of spin-Peierls order in unfrustrated antiferromagnets.[28] Note that both these spin-fluid ground states manifestly contradict Laughlin's fractional quantization principle[29] which asserts that spin-$\frac{1}{2}$ spinons must be semions.

Quantum-disordered states on the kagomé lattice were also studied by Marston and Zeng[17] by an alternative large-N method which involved the use of fermionic variables. They found spin-Peierls ordering in their ground state. The fermionic large-N limit they used generically leads to dimerization[31] and is properly considered an "extreme quantum" limit.[27] The approach of this paper allows one to approach the classically ordered phase[28] and is expected to more accurately describe the nearby quantum-disordered phases. An alternative test for the appearance of spin-Peierls order is to examine a quantum-dimer[32] model on the kagomé lattice; natural off-diagonal terms in the dimer model are interchanges of dimers around hexagons and other non-self-intersecting loops. The relationship between gauge theories derived from Sp(N) models and dual versions of the quantum dimer model[33,34] suggests that a dual version of the kagomé lattice model should be similar to the gauge theories of Sec. IV A 1. A natural conjecture then is that this quantum-dimer model has a spin-fluid ground state.

Zeng and Elser[16] have presented exact numerical diagonalizations of finite clusters of the kagomé lattice which indicate that the spin-$\frac{1}{2}$, SU(2) antiferromagnet has a quantum-disordered ground state. The specific heat of the model also displayed a double-peak structure as a function of temperature. The first peak at $T = 0.75J$ was identified with quenching of the spin fluctuations into the subspace of near-neighbor singlet bonds (dimers) and it was suggested that the second peak could possibly be associated with the appearance of spin-Peierls order. However it is not necessary for true long-range order to appear to obtain a peak in the specific heat. Further investigations involving the measurement of the appropriate correlation functions and susceptibilities is necessary before any firm conclusion on the absence of spin-Peierls order can be drawn.

Recently, Ritchey et al.[20] have suggested that the ground state of the quantum SU(2) antiferromagnet retains the degeneracy of the 3-state Potts antiferromagnet on the kagomé lattice. However, as we demonstrated explicitly in Sec. V A, quantum fluctuations break the degeneracy between these states. Moreover, it is reasonable to expect that higher-order corrections in a semiclassical theory will also lead to a splitting of the degeneracy between these states. Ritchey et al.[20] focused solely on the tunneling between the Potts-like states and ignored the possibility of diagonal shifts in the energy. It is unlikely that their ground state will survive the inclusion of these effects.

B. Magnetically ordered phases

First, we review the large-N results of this paper on the zero temperature quantum Heisenberg antiferromagnets. For large values of the "spin" we obtained magnetically ordered states. The ordering on the triangular lattice was the usual classical three-sublattice state. The kagomé lattice ordering had a $\sqrt{3} \times \sqrt{3}$ unit cell with 9 sites. We demonstrated explicitly the quantum fluctuation induced selection of this structure from among the huge manifold of classically degenerate states. The only low-lying excitations were shown to be long-wavelength spin-wave modes; there were no spin-wave modes with a vanishing energy at all wave vectors that appear in the classical limit.

Harris et al.[18] have performed a large-S expansion for the ground state of a kagomé lattice antiferromagnet with first-, second-, and third-neighbor interactions. They found regimes in which both the $\sqrt{3} \times \sqrt{3}$ and the $\mathbf{k} = 0$ states were the ground states.

Zeng and Elser[16] have discussed a large-S spin-wave calculation which interpolates between the kagomé and triangular lattices and finds a quantum-disordered state on the kagomé lattice for all S. This result therefore differs from the large-N result of this paper that the ground state is magnetically ordered at large values of κ. However, the structure of the semiclassical expansion about the classically degenerate manifold has not yet been fully worked out, and the reliability of the prediction of the absence of magnetic order at large S is questionable. A similar discrepancy also existed between the square lattice antiferromagnet with first- (J_1) and second- (J_2) neighbor interactions at the classical disorder point $J_2 = J_1/2$. The initial large-S calculations[35] predicted disorder up to $S = \infty$, while the large-N method[3,4,7] found quantum fluctuation induced order; a subsequent reanalysis of the semiclassical theory by Chubukov[5] in fact showed the presence of long-range order, consistent with the large-N approach. A complete understanding of the semiclassical theory for the kagomé lattice is clearly called for: it is clear that a partial resummation of the large-S series is necessary.

C. Classical kagomé antiferromagnet

Next we turn to the *classical* kagomé Heisenberg antiferromagnet. Our large-N expansion for this model (see the Appendix) found no broken symmetries and short-range correlations of the $\sqrt{3} \times \sqrt{3}$ state (Fig. 2) at all finite temperatures. This agrees with the high temperature expansion of Harris et al.[18] which also found that the $\sqrt{3} \times \sqrt{3}$ structure dominated the fluctuations. In the present large-N calculation, the correlation length of the $\sqrt{3} \times \sqrt{3}$ structure diverges as $\exp(c/T)$ as $T \to 0$. Chalker et al.[19] have examined the classical kagomé antiferromagnet at low temperatures by analytical and numerical techniques. Their finite-temperature results have no long-range order and presumably have short-range correlations similar to those in the present large-N theory. They also suggested from Monte Carlo results that nematic order appears as $T \to 0$ in the classical model.

Such ordering is implicit in the $\sqrt{3} \times \sqrt{3}$ ordering obtained as $T \to 0$ in the large-N limit. Monte Carlo measurements of spin-correlation functions which distinguish between nematic and Néel-type ordering require much longer to equilibrate,[36] and were not directly examined in Ref. 19.

D. Implications for experiments

1. Helium films

Elser[22] has argued that a partially filled second layer of He^3 on graphite[21] can be well described by a spin-$\frac{1}{2}$ kagomé antiferromagnet; there are however other interpretations of the experimental data.[37] The numerical calculations of the specific heat[16] were consistent with experimental results. Experimental tests for the absence of spin-Peierls ordering would be of great interest.

2. Layered oxides

The experiments on $SrCr_{8-x}Ga_{4+x}O_{19}$ (Refs. 23–25) probe a spin-$\frac{3}{2}$ kagomé lattice antiferromagnet. Interpretation of the experiments is however complicated by the presence of disorder. The powder average neutron scattering shows a broad maximum around $k = 4\pi/3a$,[25] consistent with short-range order of the $\sqrt{3} \times \sqrt{3}$ type. However, despite the presence of substantial elastic scattering indicating a static moment, the correlation length, as defined by the width of the peak at $k = 4\pi/3a$, saturates at low temperature. In particular it does not have the $\exp(c/T)$ increase expected of two-dimensional long-range-ordered states. This suggest that the static moment is random, and the ordering influenced strongly by the presence of disorder. This scenario is also supported by a large enhancement in the measured nonlinear susceptibility.

One is then left with the puzzle of understanding the low temperature behavior of the specific heat $C \sim T^2$ and the dynamic neutron scattering. The low-lying modes in a spin glass are expected to be spin waves[38] with a dispersion spectrum $\sim ck$. This leads naturally to a specific heat $\sim T^2$ in two dimensions. To determine the neutron scattering spectrum, let us consider the nature of the long-wavelength, low energy action describing the system. These will be dominated by slow distortions of a reference ground state $S_\ell^0(\mathbf{r})$:

$$S_\ell(\mathbf{r}, \tau) = R_{\ell m}(\mathbf{r}, \tau) S_m^0(\mathbf{r}) , \qquad (6.1)$$

where $\ell, m = 1, 2, 3$ are spin indices, R is a slowly varying rotation matrix, and τ is the imaginary time. We expect the action controlling Ω to be a nonlinear sigma model.[38-40] On general grounds,[41] the long-wavelength, long-time fluctuations can be well described by the following disorder-averaged correlation function at low temperatures:

$$\langle R(\mathbf{k}, \omega_n) R(-\mathbf{k}, -\omega_n) \rangle \sim \frac{1}{\omega_n^2 + c^2 \mathbf{k}^2 + \Delta^2(T)} , \qquad (6.2)$$

where the "gap" $\Delta(T) \to 0$ as $T \to 0$. In a system with a large moment at $T = 0$ we expect $\Delta \sim \exp(-c/T)$; the kagomé lattice system has a small moment and therefore may be dominated by quantum critical fluctuations, in which case $\Delta \sim T$ (Refs. 40 and 42) over a significant range of intermediate temperatures. In either case, this implies that as $T \to 0$ the local response function, $\chi_0''(\omega)$ has the form

$$\chi_0''(\omega) \sim \lim_{\eta \to 0} \int d^2\mathbf{k} \, \mathrm{Im} \left(\frac{1}{-(\omega + i\eta)^2 + c^2\mathbf{k}^2} \right)$$
$$\sim \mathrm{sgn}(\omega) . \qquad (6.3)$$

This is roughly consistent with the experimental results.

A possible objection to the above scenario is that the Halperin-Saslow spin-wave modes have not been observed in conventional 3D spin glasses because they are completely dominated by low-lying, short-wavelength excitations which have a constant density of states at low energy. Why, then, do they dominate the thermodynamics here? There are two possible reasons for this.

(i) In 3D, the specific heat from the long-wavelength modes would be $\sim T^3$ and is thus more likely to be swamped by local excitations;

(ii) the kagomé spin glass is very close to a quantum-disordered phase with a gap. This reduces the density of particularly the short-wavelength but low energy excitations, allowing the long-wavelength modes to dominate the thermodynamics.

A careful theoretical analysis of random quantum antiferromagnets on the kagomé net is necessary before the above scenario can be subjected to quantitative tests.

ACKNOWLEDGMENTS

APPENDIX: CLASSICAL KAGOMÉ HEISENBERG ANTIFERROMAGNET

In this appendix we shall show how the $Sp(N)$, large-N approach can be applied to the classical antiferromagnet on a kagomé lattice. The classical antiferromagnet is defined by the partition function

$$Z = \int \mathcal{D}\Omega \exp\left(-\frac{H_c}{T} \right) ,$$
$$\qquad (A1)$$
$$H_c = -\frac{J}{2N} \sum_{<ij>} \mathcal{J}^{\alpha\beta} \mathcal{J}_{\gamma\delta} \Omega_\alpha^\gamma(i) \Omega_\beta^\delta(j) ,$$

where $\alpha, \beta, \gamma, \delta = 1, \ldots, 2N$. The functional integral over the spin Ω is restricted to the manifold[3,4]

$$\Omega \in \frac{\mathrm{Sp}(N)}{\mathrm{Sp}(N-1) \times \mathrm{U}(1)} \tag{A2}$$

on every site i; there is no time dependence. The dimension of $\mathrm{Sp}(N)$ is $2N^2 + N$, so the dimension of the manifold of Ω can be determined from (A2) to be $4N - 2$. A simple way to realize this manifold is to introduce the $2N$ complex numbers z^α [which transform as $\mathrm{Sp}(N)$ spinors] and restrict

$$\Omega_\alpha^\beta = z_\alpha^* z^\beta \, , \quad \sum_\alpha |z^\alpha|^2 = N \, , \tag{A3}$$

on every site of the lattice. As Ω is invariant under the gauge transformation $z^\alpha \rightarrow e^{i\rho} z^\alpha$, the dimension of the manifold so realized is also $4N - 2$.

The large-N expansion of the classical antiferromagnet can be obtained directly from the expressions (A1): the analysis parallels that of Sec. II but with the operators b_i^α replaced by the complex numbers z^α. However, it is quicker, and also instructive, to extend the quantum theory of Sec. IV to finite T and take the limit of large κ: identical results are obtained. Since the energies increase as κ^2 for large κ it is necessary to scale T by κ^2 in taking this limit.

Generalizing the expression (4.7) to finite temperature, we obtain the following large-N result for free energy of the kagomé-lattice quantum antiferromagnet at a finite temperature T:

$$\frac{F_{\mathrm{MF}}}{NN_s} = \frac{1}{N_s} \sum_{\mathbf{k},\mu} [\omega_\mu(\mathbf{k}) + 2T \ln(1 - e^{-\omega_\mu(\mathbf{k})/T})]$$
$$+ \frac{J}{2}(|Q_1|^2 + |Q_2|^2) - \lambda(1 + \kappa) \, , \tag{A4}$$

where the eigenfrequencies $\omega_\mu(\mathbf{k})$ are given by Eqs. (4.4), (4.5), and (4.6). We take the classical limit of this result by first performing the following rescalings:

$$T \rightarrow \kappa^2 T \, , \quad Q \rightarrow 2\kappa T Q/J \, , \quad \lambda \rightarrow \kappa T \lambda \, , \quad \omega_\mu \rightarrow \kappa T \omega_\mu \, , \tag{A5}$$

and then taking the large-κ limit. The leading term in the quantum free energy F_{MF} is the classical result F_c:

$$\frac{F_c(Q, \lambda)}{NN_s T} = \frac{2}{N_s} \sum_{\mathbf{k},\mu} \ln[\omega_\mu(\mathbf{k}, Q, \lambda)]$$
$$+ \frac{2T}{J}(|Q_1|^2 + |Q_2|^2) - \lambda \, . \tag{A6}$$

We have explicitly displayed the dependence of ω_μ on the variational parameters Q, λ. This result can also be obtained by a direct large-N analysis on the partition function in Eq. (A1). As expected, dependence on κ has now disappeared, and all results depend only on the value of T/J.

We numerically minimized F_c with respect to the complex numbers Q_1 and Q_2, subject to the constraint

$$\frac{\partial F_c}{\partial \lambda} = 0 \, . \tag{A7}$$

As in Sec. IV A, the optimum configuration always satisfied $Q_1 = -Q_2$. This indicates the presence of short-range correlations with the structure of the $\sqrt{3} \times \sqrt{3}$ state (Fig. 2); the correlation length diverges as $\exp(c/T)$ as $T \rightarrow 0$. All other values of Q lead to states with higher energies.

The structure factor of the $Q_1 = -Q_2$ classical state was determined by taking the classical limit of Eq. (2.18), and the result is shown in Fig. 6 for $T/J = 0.225$. We have rescaled the spin variables by a factor $2/\kappa$, and from Eq. (2.19) the structure factor therefore satisfies the sum rule

$$\frac{1}{N_s} \sum_{\mathbf{k}} S(\mathbf{k}) = 1 \, . \tag{A8}$$

Finally we examine the nature of the zero-temperature limit $T \rightarrow 0$. From the minimization of Eq. (A6) it is not difficult to show that

$$\lambda(T \rightarrow 0) = \frac{3J}{2T} \, , \quad |Q(T \rightarrow 0)| = \frac{\sqrt{3}J}{4T} \, , \tag{A9}$$

where the second equation is satisfied by the Q_{ij} on all links. The spin-correlation length ξ obeys

$$\xi^{-2}(T \rightarrow 0) \sim T(\lambda - 2\sqrt{3}|Q|) \sim \exp(-cJ/T) \tag{A10}$$

for some constant c. The zero-temperature limit of the free energy can be obtained by inserting the above results into (A6) and by using the homogeneous, linear dependence of ω_μ on Q and λ:

$$\omega_\mu(\mathbf{k}, xQ, x\lambda) = x\omega_\mu(\mathbf{k}, Q, \lambda) \, . \tag{A11}$$

The result is

$$\lim_{T \rightarrow 0} \frac{F_c}{NN_s T} = -\frac{3J}{4T} + 2\ln(3J/2T)$$
$$+ \frac{2}{N_s} \sum_{\mathbf{k},\mu} \ln\{\omega_\mu[\mathbf{k}, \pm 1/(2\sqrt{3}), 1]\} \, . \tag{A12}$$

In the last term we evaluate ω_μ from Eqs. (2.6) and (2.12) or equivalently from Eqs. (4.4)–(4.6) with $\lambda = 1$, $Q_1 = -Q_2$, and $|Q_1| = |Q_2| = 1/(2\sqrt{3})$.

In a very similar manner we could have examined the zero-temperature limit of the free energy of thermal fluctuations around any of the coplanar configurations considered in Sec. V A. The only difference from the above analysis would have been that instead of choosing $Q_1 = -Q_2$, the link variables Q_{ij} would all be equal in magnitude but differ in their signs; the manner in which each state of the Potts antiferromagnet can be associated with a particular set of assignments of the signs of the Q_{ij} was discussed in Sec. V A. The eigenfrequencies ω_μ would be determined by solving Eqs. (2.6) and (2.12). The zero-temperature limit of the free energy of any of these configurations is given by an expression identical to Eq. (A12); the first two terms in (A12) are identical for

all the states but the last term involving the sum over the bosonic eigenmodes breaks the degeneracy. Thus the free energy, F_c/T, of these states will differ by a term of order N, but independent of T, as $T \to 0$. We have evaluated the zero-temperature limit of the free energy, F_c/T, of all configurations associated with the 120 ground states of the Potts antiferromagnet which are periodic with the unit cell of Fig. 15; this calculation is quite analogous to that in Sec. V A. We found that the $\sqrt{3} \times \sqrt{3}$ structure of Fig. 15(a) had the lowest free energy. As the

free energy has a prefactor N, the partition function will therefore be completely dominated by the contribution of the $Q_1 = -Q_2$ state and the $T \to 0$ limit will possess the correlations of the $\sqrt{3} \times \sqrt{3}$ structure in Figs. 15(a) or 2.

It is interesting that this state selection is quite similar to that due to quantum fluctuations discussed in Sec. V A. The only difference is that while quantum fluctuations broke the degeneracy by the term $\sum_{\mathbf{k},\mu} \omega_\mu(\mathbf{k})$, classical fluctuations do so by $\sum_{\mathbf{k},\mu} \ln[\omega_\mu(\mathbf{k})]$.

[1] M.P. Gelfand, R.R.P. Singh, and D.A. Huse, Phys. Rev. B 40, 10 801 (1989); M.P. Gelfand, *ibid.* 42, 8206 (1990).

[2] F. Figueirido, A. Karlhede, S. Kivelson, S. Sondhi, M. Rocek, and D.S. Rokhsar, Phys. Rev. B 41, 4619 (1990).

[3] N. Read and S. Sachdev, Phys. Rev. Lett. 66, 1773 (1991).

[4] S. Sachdev and N. Read, Int. J. Mod. Phys. B 5, 219 (1991).

[5] A. Chubukov, Phys. Rev. B 44, 392 (1991).

[6] S. Sachdev and R.N. Bhatt, Phys. Rev. B 41, 4502 (1990).

[7] F. Mila, D. Poilblanc, and C. Bruder, Phys. Rev. B 43, 7891 (1991).

[8] E. Dagotto and A. Moreo, Phys. Rev. Lett. 63, 2148 (1989); R.R.P. Singh and R. Narayan, *ibid.* 65, 1072 (1990); A. Moreo, E. Dagotto, T. Jolicoeur, and J. Riera, Phys. Rev. B 42, 6283 (1990); T. Ziman and H. Schulz (unpublished).

[9] X.-G. Wen, F. Wilczek, and A. Zee, Phys. Rev. B 39, 11 413 (1989).

[10] D.A. Huse and V. Elser, Phys. Rev. Lett. 60, 2531 (1988).

[11] D. Yoshioka and J. Miyazaki, J. Phys. Soc. Jpn. 60, 614 (1991); A. Kol and N. Read (unpublished).

[12] V. Kalmeyer and R.B. Laughlin, Phys. Rev. Lett. 59, 2095 (1987).

[13] P. Chandra and P. Coleman, Phys. Rev. Lett. 66, 100 (1991).

[14] P.W. Anderson, Science 235, 1196 (1987).

[15] J. Villain, R. Bidaux, J.P. Carton, and R. Conte, J. Phys. (Paris) 41, 1263 (1980); E. Shender, Zh. Eskp. Teor. Fiz. 83, 326 (1982) [Sov. Phys. JETP 56, 178 (1982)]; E. Rastelli and A. Tassi, J. Phys. C 20, L303 (1987); C. Henley, Phys. Rev. Lett. 62, 2056 (1989).

[16] C. Zeng and V. Elser, Phys. Rev. B 42, 8436 (1990).

[17] J.B. Marston and C. Zeng, J. Appl. Phys. 69, 5962 (B) (1991).

[18] A.B. Harris, C. Kallin, and A.J. Berlinsky, Phys. Rev. B 45, 2899 (1992).

[19] J.T. Chalker, P.C.W. Holdsworth, and E.F. Shender, Phys. Rev. Lett. 68, 855 (1992).

[20] I. Ritchey, P. Coleman, and P. Chandra (unpublished).

[21] D.S. Greywall, Phys. Rev. B 41, 1842 (1990).

[22] V. Elser, Phys. Rev. Lett. 62, 2405 (1990).

[23] X. Obradors, A. Labarta, A. Isalgué, J. Tejada, J. Rodriguez, and M. Pernet, Solid State Commun. 65, 189 (1988).

[24] A.P. Ramirez, G.P. Espinosa, and A.S. Cooper, Phys. Rev. Lett. 64, 2070 (1990).

[25] C. Broholm, G. Aeppli, G. Espinosa, and A.S. Cooper, Phys. Rev. Lett. 65, 3173 (1990).

[26] D.P. Arovas and A. Auerbach, Phys. Rev. B 38, 316 (1988); Phys. Rev. Lett. 61, 617 (1988).

[27] N. Read and S. Sachdev, Nucl. Phys. B316, 609 (1989).

[28] N. Read and S. Sachdev, Phys. Rev. Lett. 62, 1694 (1989); Phys. Rev. B 42, 4568 (1990).

[29] R.B. Laughlin, Science 242, 525 (1988).

[30] E. Fradkin and S.H. Shenker, Phys. Rev. D 19, 3682 (1979).

[31] D.S. Rokhsar, Phys. Rev. B 42, 2526 (1990).

[32] D. Rokhsar and S. Kivelson, Phys. Rev. Lett. 61, 2376 (1988).

[33] E. Fradkin and S. Kivelson, Mod. Phys. Lett. B4, 225 (1990).

[34] R. Jalabert and S. Sachdev, Phys. Rev. B 44, 686 (1991); N. Read and S. Sachdev (unpublished).

[35] P. Chandra and B. Doucot, Phys. Rev. B 38, 9335 (1988).

[36] D. Huse and A.D. Rutenberg (unpublished).

[37] M. Roger, Phys. Rev. Lett. 64, 297 (1990); K. Machida and M. Fujita, Phys. Rev. B 42, 2673 (1990).

[38] B.I. Halperin and W.M. Saslow, Phys. Rev. B 16, 2154 (1977).

[39] T. Dombre and N. Read, Phys. Rev. B 39, 6797 (1989).

[40] P. Azaria, B. Delamotte, and T. Jolicoeur, Phys. Rev. Lett. 64, 3175 (1990); P. Azaria, B. Delamotte, and D. Mouhanna (unpublished).

[41] A.M. Polyakov, *Gauge Fields and Strings* (Harwood, New York, 1987).

[42] S. Chakravarty, B.I. Halperin, and D.R. Nelson, Phys. Rev. Lett. 60, 1057 (1988); Phys. Rev. B 39, 2344 (1989).